SSD

SCIENCE FOR A SUSTAINABLE DEVELOPMENT

FINAL REPORT PHASE I

CLIMATE CHANGE IMPACT ON HYDROLOGICAL EXTREMES ALONG RIVERS AND URBAN DRAINAGE SYSTEMS IN BELGIUM «CCI-HYDR»

V. NTEGEKA, P. WILLEMS, P. BAGUIS, E. ROULIN

ENERGY

TRANSPORT AND MOBILITY

AGRO-FOOD

HEALTH AND ENVIRONMENT

CLIMATE

BIODIVERSITY

ATMOSPHERE AND TERRESTRIAL AND MARINE ECOSYSTEMS

TRANSVERSAL ACTIONS

.be

SCIENCE FOR A SUSTAINABLE DEVELOPMENT
(SSD)

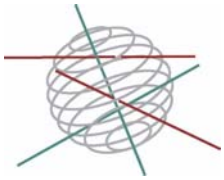

Climate

FINAL REPORT PHASE I

CLIMATE CHANGE IMPACT ON HYDROLOGICAL EXTREMES ALONG RIVERS AND URBAN DRAINAGE SYSTEMS IN BELGIUM
«CCI-HYDR»

SD/CP/03A

Promotors
Patrick Willems
Katholieke Universiteit Leuven (K.U.Leuven)
Faculty of Engineering
Department of Civil Engineering
Hydraulics Section
Kasteelpark Arenberg 40
B-3001 Heverlee (Leuven)
Tel: +32 (0)16 321658
Fax: +32 (0)16 321989
Patrick.Willems@bwk.kuleuven.be
www.kuleuven.be/hydr

Emmanuel Roulin
Royal Meteorological Institute of Belgium (RMI)
Meteorological Research and Development Department
Risk Analysis and Sustainable Development Section

Authors
Victor Ntegeka, Patrick Willems (KULeuven)
Pierre Baguis, Emmanuel Roulin (RMI)

April 2008

BELGIAN SCIENCE POLICY

KATHOLIEKE UNIVERSITEIT LEUVEN

RMI

Rue de la Science 8
Wetenschapsstraat 8
B-1000 Brussels
Belgium
Tel: +32 (0)2 238 34 11 – Fax: +32 (0)2 230 59 12
http://www.belspo.be

Contact person:
Mrs Sophie Verheyden
Secretariat: +32 (0)2 238 36 12
Project website : http://www.kuleuven.be/hydr/CCI-HYDR.htm

Victor Ntegeka, Patrick Willems, Pierre Baguis, Emmanuel Roulin. ***Climate change impact on hydrological extremes along rivers and urban drainage systems in Belgium «CCI-HYDR»*** Final Report Phase 1. Brussels : Belgian Science Policy 2009 – 45 p. (Research Programme Science for a Sustainable Development)

Table of contents

1 Introduction

1.1 The CCI-HYDR project

With the advent of new advances in climate science, climate models have morphed from Global Circulation Models (GCMs) to Regional Circulation Models (RCMs). This has opened up new research opportunities for impact analysts interested in small scale regional impacts. The CCI-HYDR project was supported by the Belgian Science Policy Office through their Science for Sustainable Development programme to exploit the latest data from the new climate change models. The key aim of the project was to investigate the climate change impact on the risk of hydrological extremes along rivers and urban drainage systems in Belgium. The research was primarily based on results from the high resolution PRUDENCE regional climate models and later extended to include the GCM models from the Fourth Assessment Report (AR4) of the United Nations Intergovernmental Panel on Climate Change (IPCC). The climate models from the PRUDENCE project were arguably among the first models that were primarily set up to investigate regional impacts. The collaborations from various modelling centres and climate experts also increased confidence in the use of the outputs from the project. The PRUDENCE project also made a substantial contribution to the latest IPCC AR4 report. The CCI-HYDR project engaged a collaborative team of meteorological, hydrological and water engineering researchers from the Katholieke Universiteit Leuven and the Royal Meteorological Institute (RMI) of Belgium. However, a collaboration was also arranged with the ADAPT project, which is responsible for examining the wider implications of the CCI-HYDR outcomes to the society, water managers, and policy makers.

1.2 Context

Flood risk is in Belgium as well as in other European countries of considerable importance especially due to the dense populations and high industrialization along the river banks. Also, since the last decades, sewer systems are being built at large scale. Drought risks are less significant in the country, due to the humid climate and the limited length of the dry spells in summer. However, extreme low flows may occur along rivers, causing severe problems of water shortage for drinking water supply, for agriculture and for the environment.

There is strong evidence that due to global climate change, the risks of inundations and low flows are changing. Water managers have to anticipate these changes so as to limit the flood and drought risks of the inhabitants to acceptable risk levels. In addition to the water administrations, the insurance industry needs quantification of their related risks, as well as the different water users, and policy makers so as to develop and adapt policies (e.g. CO_2 emission reduction).

The concerns about the impact of climate change on the hydrological water cycle (including floods and droughts) have triggered specific studies since the 1980s. RMI has been pioneering in putting into evidence differences in the sensitivity of catchments with contrasted characteristics to a $2xCO_2$ scenario (e.g. Bultot et al. [1988]). They extended their study to a larger set of catchments and used the first set of climate change scenarios made available by IPCC [Gellens and Roulin, 1998]. The scope was further extended to the whole Meuse river basin [Roulin et al., 2001] and Scheldt river basin [Roulin and Arboleda, 2002] using a new set of climate scenarios based on transient experiments, for instance based on the results of Global Circulation Models (GCMs) forced with an increasing greenhouse gas content. However, the GCMs have since improved, and high resolution regional climate models have been nested within to downscale the climate variables to regional scale. This has sparked new research related to regional impacts relevant at local scales. Hydrological impact assessments can now be performed with increased confidence.

Through analysis of seasonal precipitation anomalies and low flow indicators, de Wit et al. [2007] have shown that multi-seasonal droughts had generated severe low flows in the river Meuse in 1921 and 1976. These authors did not find an increase of occurrence of such multi-seasonal drought in the results of the regional climate change simulation of the PRUDENCE project (e.g. Räisänen et al. [2004]). Instead, there was a large increase of the occurrence of extremely dry summers. The impact of such scenarios on the discharges of Belgian rivers deserves further detailed investigation with the use of hydrological and hydrodynamic models.

1.3 Project objectives

The CCI-HYDR research project was set up to investigate in a detailed objective way and based on the most recent data and climate modelling results, the climate change impact on the risk of hydrological extremes along rivers and urban drainage systems in Belgium. To accomplish the project objectives, the research was subdivided into two phases. Phase 1 of the project focused on the selection of the RCM scenarios and the long-term historical investigation of rainfall and evapotranspiration. Climate change scenarios were developed for both rainfall (including extreme conditions) and ETo. In Phase 2 of the project, the implications of the scenarios on the hydrological extremes will be studied. This involves investigation of flood and low flow risks along rivers and flood risks along selected urban drainage systems in Belgium. The project results will provide useful additional support for policy development especially related to sustainable development such as the Kyoto Protocol.

1.4 Overview of methodology

The study required a comprehensive assessment of the state-of-the-art climate model data relevant for hydrological impact analysis. Thus, there was a need for investigating the historical trends from the observed series and the future predictions from the most recent regional climate models. The latter was accomplished by evaluating the RCM model outputs relevant to the hydrological impact through statistical tests while the former was studied by applying a trend analysis technique that combines the frequency and magnitude of extremes.

The historical trend analysis was performed for both the potential reference evapotranspiration (ETo) and rainfall series. Each of the available time series was long enough (greater than 100 years) for a realistic assessment for existing trends. A unique 10-minute rainfall series for the period 1898-2005 was made available by IRM including a daily ETo series for the period 1901-2005. A technique that derives the temporal changes in the magnitudes of extremes and tests for their statistical significance was developed for the trend analysis. The technique was used to identify the anomalous periods within the observed time periods. The historical trends would also provide a basis for verifying the consistencies of the climate model predictions for the future changes. Models can only produce credible projections if they succeed to simulate realistic future trends consistent with the past (observed) trends. The future trends may be projected backwards towards the observed trends. If a portion of the observed trends is not within the projection, the model is biased for trends. This would implicitly be linked to the errors in the internal dynamics or physics of the climate model which would suggest down-weighting or exclusion of the model from the selected group.

The evaluation of the RCMs was achieved through statistical tests and visual interpretation of the related outputs. The RCMs were evaluated against the observed measurements for the consistency in mean statistics, seasonality, spatial variability, inter-annual variability, and trends. The CCI-HYDR project primarily focused on the regional results from the PRUDENCE project. The latter provides high-resolution data (12-50km) over Europe for both the observed climate (1961-1990) and the future climate at the end of the twenty-first century (2071-2100). In particular, the study evaluated outputs with direct relevance to hydrological impacts such as rainfall and ETo. Unlike rainfall which is provided as a direct output from the climate models ETo is not directly available. Instead, it is derived from other inputs: wind speed, humidity, cloud covering, pressure, temperature, and radiation. However, only temperature and rainfall were extensively tested due to the scant data for other observed variables. The models were also tested for their performance at a regional scale. An areal performance measure enabled the identification of models which on average had significant errors over the Belgian region. The combination of areal and point performance measures of the regional climate models led to a selection of climate models suitable for the Belgian climate.

The local and spatial assessment culminated in the selection of climate models for hydrological impact modelling. The selected climate models can now be used for climate change studies in Belgium with increased confidence. It is notable that despite the dynamic downscaling of the selected RCMs, there was still a need for further downscaling. The statistical evaluations of the PRUDENCE model results revealed that the direct use of the biased model results would subsequently lead to biased impact analysis. Even so, the large set of models implied that the interpretations would be difficult for the impact analysts. Therefore, three scenarios were identified which would simplify the interpretation and at the same time account for the overall uncertainty from the selected models. The three scenarios were deduced through a statistical downscaling method that involved the transfer of the changes estimated from the climate models to an observed time series. The changes were mainly considered

to be within the number of wet days and the intensities of the wet days. Based on the entire set of the models the high, mean and low scenario cases were selected to represent the overall expected range of changes. These were extracted from a probabilistic analysis of the entire set of the model projections.

The three-case scenario approach was then used to transform the observed series of rainfall and ETo which are the key factors for impact modelling in hydrological lumped conceptual models. Lumped conceptual models are preferred to distributed models for testing the downscaling methodology due to the short computation times, which makes them suitable for simulating various downscaled time series. In essence, the three cases are finalised after a series or trials which entail perturbing the rainfall and ETo series and checking the outputs against the overall range of expected impacts. The final flow outcomes from three scenarios that are categorised as high, mean, and low should match the range that would have been simulated if all the selected models were simulated. The high case defines the most extreme scenario (highest flow impact) which corresponds to the most severe case for flood risk analysis. The mean case represents the expected average scenario (mean flow impact) while the low scenario (lowest flow impact) in contrast to the high scenario reflects the most severe low flow situation. However, since the PRUDENCE RCM models were based on only the A2 and B2 future greenhouse gas emission scenarios [IPCC, 2001], scaling factors were required to make the scenarios more exhaustive by including changes from extra scenarios (notably the A1B and B1). These were derived from the IPCC AR4 models.

The developed climate change scenarios are crucial for impact studies. Also, ecological impact assessments benefit from the outputs of the hydrological-hydrodynamic models which are based on the generated scenarios. The impact results can also support the study of adaptation measures.

Based on the statistically probed scenarios, the CCI-HYDR project Phase 1 would have provided scenarios which are constructed specifically for the Belgian climate. The methodology is described in detail in the next sections. It is important to keep in mind that the detailed descriptions are presented based on the studies during the project Phase 1 and more details will be made available during Phase 2 of the project while studying the impacts of the climate change scenarios on the hydrodynamics of rivers and urban drainage systems in Belgium.

2 Database for the CCI-HYDR project

2.1 Historical trend data

For a more conclusive study of trends the project required long records of rainfall and ETo. Fortunately, IRM/KMI has produced a long-term high-frequency homogeneous rainfall series at the climatological station of Uccle that starts in 1898 and which is continued to date; data for the period 1898-2005 was used for this project. Also, a long term series for ETo based on the Bultot [1983] method was available for the period 1901-2005. The long periods enable the tracing of systematic and persistent patterns within the observed series. Phase 1 of the project focused on the two long series for the trend analysis. However, longer records for discharge will also be investigated at a later stage.

2.2 The PRUDENCE RCM database

The PRUDENCE project produced regional climate change scenarios specifically for Europe and was consequently chosen as the main source of climate change scenarios. PRUDENCE is an acronym for Prediction of Regional scenarios and Uncertainties for Defining EuropeaN Climate change risks and Effects (e.g. Räisänen et al., 2004; Christensen, 2005; Christensen et al., 2007). It is a project with many European partners, funded by the EU 5th Framework Program and having as goal the evaluation of climate change risks over Europe in the end of the current century, as predicted by the most recent (at the project time) climate models. The project applied dynamic downscaling to generate climate data at small scales (12-60km). The PRUDENCE project carried out a series of 30-year long climate simulations for the reference period (1961-1990) and at the end of the 21st century (2071-2100). The models were run using A2 and B2 SRES scenarios (IPCC, 2001) and coupled with two Atmosphere Ocean Global Circulation Models (AOGCMs). The results of these simulations were then used to drive geographically more detailed RCM-based simulations (11 RCMs in total). The project ended in 2004 and at its end, the simulation data from its participants were freely available in public domain of the project host (http://prudence.dmi.dk). Due to the detailed and thorough data available, based on many climate models and covering the whole European continent including Belgium. The results of these simulations were used in the present study.

Table 1 shows the 21 PRUDENCE control experiments (1961-1990) that were used. Table 2 shows the 31 RCM scenarios (2071-2100) for the future projections.

2.3 GCM data from the IPCC AR4 database

The GCM experiments were required to account for the extra uncertainty related to emission scenarios. However, given the differences in priorities, the IPCC AR4 models would not necessarily fit the same criteria for the CCI-HYDR project analysis; the control and scenario periods of the AR4 GCMs do not in general coincide with those of the PRUDENCE RCMs. Nonetheless, many of the GCMs fit the criteria which allows for checking the estimated PRUDENCE projections which were only based on the A2 and B2 scenarios. Table 3 shows the GCMs that were used from the AR4 GCM database (http://www.ipcc-data.org).

Table 1: PRUDENCE control series (1961-1990) used in the project.

PRUDENCE PARTNER	MEMBER	CONTROL	GCM	RCM
Météo France (France)	CNRM	DA9	Observed SST	ARPEGE
Danish Meteorological Institute (Denmark)	DMI	ECC	ECHAM5	HIRHAM
		ecctrl	ECHAM4/OPYC	HIRHAM
		HC1	HadAM3H	HIRHAM
		HC2	HadAM3H	HIRHAM
		HC3	HadAM3H	HIRHAM
		F25	HadAM3H	HIRHAM
Swiss Federal Institute of Technology (Switzerland)	ETH	HC_CTL	HadAM3H	CHRM
GKSS Forschungszentrum Geesthacht GmbH (Deutschland)	GKSS	CTL	HadAM3H	CLM
		CTLsn	HadAM3H	CLM (improved)
Met. Office Hadley Centre (United Kingdom)	HC	adeha	HadAM3P	HadRM3P
		adehb	HadAM3P	HadRM3P
		adehc	HadAM3P	HadRM3P
The Abdus Salam Intl. Centre for Theoretical Physics (Italy)	ICTP	ref	HadAM3H	RegCM
Koninklijk Nederlands Meteorologisch Instituut (The Netherlands)	KNMI	HC1	HadAM3H	RACMO
Norwegian Meteorological Institute (Norway)	METNO	HADCN	HadAM3H	HIRHAM
Max-Planck-Institut für Meteorologie (Deutschland)	MPI	3003	HadAM3H	REMO
Swedish Meteorological and Hydrological Institute (Sweden)	SMHI	HCCTL	HadAM3H	RCAO
		MPICTL	ECHAM4/OPYC	RCAO
		HCCTL_22	HadAM3H	RCAO (High res.)
Universidad Complutense de Madrid (Spain)	UCM	control	HadAM3H	PROMES

Table 2: PRUDENCE scenario series (2071-2100) used in the project.

MEMBER	SCENARIO	RESOLUTION (Km)	SCENARIO	GCM	RCM
SMHI	SMHI-MPI-A2	49	A2	ECHAM4/OPYC	RCAO
	SMHI-MPI-B2	49	B2	ECHAM4/OPYC	
	SMHI-HC-22	24	A2	HadAM3H	
	SMHI-A2	49	A2	HadAM3H	
	SMHI-B2	49	B2	HadAM3H	
KNMI	KNMI	47	A2	HadAM3H	RACMO
METNO	METNO-A2	53	A2	HadAM3H	HIRHAM
	METNO-B2	53	B2	HadAM3H	
DMI	DMI-S25	25	A2	HadAM3H	HIRHAM
	DMI-ecsc-A2	50	A2	ECHAM4/OPYC	
	DMI-ecsc-B2	50	B2	ECHAM4/OPYC	
	DMI-HS1	50	A2	HadAM3H	
	DMI-HS2	50	A2	HadAM3H	
	DMI-HS3	50	A2	HadAM3H	
ETH	ETH	55	A2	HadAM3H	CHRM
HC	HC-adhfa	50	A2	HadAM3P	HadRM3P
	HC-adhfe	50	A2	HadAM3P	
	HC-adhff	50	A2	HadAM3P	
	HC-adhfd-B2	50	B2	HadAM3P	
MPI	MPI-3005	55	A2	HadAM3H	REMO
	MPI-3006	55	A2	HadAM3H	
CNRM	CNRM-DC9	59	A2	ARPEGE	ARPEGE
	CNRM-DE5	59	A2	ARPEGE	
	CNRM-DE6	59	A2	ARPEGE	
	CNRM-DE7	59	A2	ARPEGE	
GKSS	GKSS-SN	55	A2	HadAM3H	CLM
	GKSS	55	A2	HadAM3H	CLM
ICTP	ICTP-A2	52	A2	HadAM3H	RegCM
	ICTP-B2	52	B2	HadAM3H	RegCM
UCM	UCM-A2	52	A2	HadAM3H	PROMES
	UCM-A2	52	B2	HadAM3H	

Table 3: GCM experiments from the AR4 GCM database (IPCC Data Distribution Centre)

Centre	Model	Control	A2	A1B	B1
BCCR	BCM2.0	•			•
CCCma	CGCM3 (T47)	•		•	•
CNRM	CM3	•	•	•	•
CSIRO	Mk3.0	•	•	•	•
MIUB, METRI, M&D	ECHO-G	•	•	•	
LASG	FGOALS-g1.0			•	
GFDL	CM2.0		•	•	•
	CM2.1		•	•	•
GISS	AOM	•		•	•
	E-H	•		•	
	E-R	•	•		
INM	CM3.0	•		•	
IPSL	CM4	•	•	•	•
NIES	MIROC3.2 hires			•	•
	MIROC3.2 medres		•	•	•
MRI	CGCM2.3.2	•	•	•	•
NCAR	PCM		•	•	
	CCSM3		•	•	•
UKMO	HadCM3	•	•	•	•
	HadGEM1	•	•	•	

3 Statistical analysis of trends and cycles

3.1 Introduction

Long-term temporal analysis of trends and cycles is essential in understanding the natural variability within the climate system [Türkes et al., 2002]. The long-term historical series can also be used to project future behaviour, and to reconstruct paleoclimatic data [Casty et al., 2005]. Investigation was made on whether the recent historical changes in frequency and amplitude of rainfall extremes can be considered statistically significant under the hypothesis of no trend or temporal clustering of rainfall extremes. The analysis was based on a 108-year time series of 10-minute Peaks-Over-Threshold (POT) rainfall data obtained from the Uccle station in Belgium.

Previous studies have examined the Uccle series albeit with varying record length, statistical properties and different analytical tools. The existence of trends and cycles based on previous studies has been somewhat unclear. Vaes et al. [2002] examined the trends in the Uccle precipitation (1898-1997) based on POT values and found no significant persisting trends. The most recent period (last 7 years) was not included. They used linear trend assumptions for the number of rainfall extremes over time. De Jongh et al. [2006] studied the trends and cycles in the precipitation record for Uccle for a 105 years time span using the Mann-Kendall trend test and wavelet analysis. Statistically insignificant trends were identified in the annual total precipitation, winter total precipitation (December, January, February), and the monthly total precipitation. The wavelet analysis did not reveal dominant periodic cycles in the monthly volumes over time. Blanckaert and Willems [2006] conducted a spectral analysis based on Fast and Windowed Fourier Analysis and wavelet analysis based on the hourly series for the period 1898 - 2001. It was concluded that there were no dominant cycles in the rainfall extremes, possibly due to the high noise - signal ratio (strong natural variability in the rainfall extremes).

The trend and cycle historical characteristics were assessed through an alternative method based on frequency-perturbations or quantile-perturbations of extremes [Ntegeka and Willems, 2008]. While frequency techniques focus on how often an event (a quantile) may occur, perturbation techniques determine the relative magnitudes of events based on a certain baseline. The frequency- or quantile-perturbation analysis compounds the two concepts thereby making it possible to study the changes in the extremes for particular return periods. This approach provides an insightful temporal assessment of the trends and oscillations of rainfall extremes. The CCI-HYDR project mainly focused on the changes in extremes. Thus, the historical assessment primarily studied the changes in the peaks. In other words by observing the changes in the POT values, it is possible to identify changes pertinent to the extremes.

3.2 Quantile-perturbation

The quantile-perturbation method investigates the historic changes in the ranked extremes. The method combines aspects of frequency, used in extreme value analysis, and perturbation, used in climate change impact studies. The perturbation factors are calculated as ratios of two similarly ranked values obtained from the future (climate model scenarios) and the observed time series (control series). The method, however, is solely based on historical data although it is applicable to climate change assessments that depend on historical and future data.

The perturbation factor is based on nearly independent extremes extracted from the long-term series and it reflects anomalies in extreme value quantiles (extremes for given empirical probabilities of being exceeded or for given mean recurrence intervals). They are calculated for subperiods (called block periods with given block size) of the full available long-term series. All extremes in a block period are compared with the corresponding quantiles derived from the full series. The mean factor difference (called “perturbation factor”) is calculated for all quantiles above a specific mean recurrence interval of 0.1 years. These quantiles reflect the most extreme conditions in the series. They correspond for rainfall to the most extreme rain storms in the series: the ones that induce flooding along rivers and sewerage systems. Block sizes of 5 to 15 years were considered and the analysis was made based on the four climatological seasons. For time scales higher than the time step of the series, perturbations are calculated from the aggregated series. For instance for the Uccle series of 10-minute rainfall intensities, aggregation times considered were 10 minutes, 1 hour, 1 day, 1 week and 1 month (using a moving average procedure with a moving step of 10 minutes). Because changes in extreme

rainfall quantiles might be explained by both changes in the number of extreme rainfall events and changes in the rainfall intensity per event, perturbation factors were derived for each of these variables.

The quantile perturbation calculation starts from a series with a given time step (e.g. 10 minutes, monthly) and a length of L years from which nearly independent rainfall extremes are extracted. Rainfall extremes are defined as nearly independent when they are separated by a time span of at least 12 hours. It follows that for aggregation times higher than 12 hours, independent extremes are separated by a time span equal to or greater than the aggregation time. The extremes after ranking represent quantiles x(L/i) with empirical recurrence intervals L/i, where i is the rank number (1 for the highest). The full series thereafter is divided in block periods with fixed block size L_b, moving from the first to the last block with a moving step of 1 year. When the quantiles present in each block period are denoted $x_b(L_b/i_b)$, where i_b is the rank number (1 for the highest in the block period), and the perturbation factor of each of these quantiles is calculated by dividing it with $x(L_b/i_b)$. When L_b/i_b does not match one of the L/i recurrence intervals, closest L/i is considered. After averaging the perturbation factors for all recurrence intervals higher than 0.1 years the mean perturbation in extreme quantiles is derived per block period. It is plotted at the central time moment of the block period. Results in Figure 1 and Figure 2 represent the temporal variability in extreme quantile perturbations, for block periods sliding with a 1 year step. A perturbation factor of 1.1 plotted for a given time moment means that extreme rainfall quantiles in the block period centred around this time moment are on average 10% higher in comparison with the long-term average (perturbation factor 1). By analyzing the block periods, multidecadal variability is isolated from higher frequency fluctuations such as internal or decadal variability.

The significance testing is based on 95% confidence intervals on the perturbation factors calculated under the hypothesis of randomness (no trend, no serial dependence or persistence) of the extremes, and making use of extreme value distributions derived for the historical observations in the full series. From these distributions, 1000 random samples are generated. The 25th and 975th sample values after ranking define the 95% confidence intervals.

3.3 Rainfall historical trends and cycles

The analysis was carried out for the four climatological seasons: winter (December, January and February), spring (March, April, May), summer (June, July, August) and autumn (September, October and November). Based on the Uccle series and the perturbation factor in extreme rainfall quantiles, oscillations are observed (Figure 1) with higher extreme rainfall quantiles in the 1910s-1920s, the 1960s and recently during the past 15 years. Lower extreme rainfall quantiles are observed in the 1930s-1940s, and in the 1970s. During the past 108 years, the multidecadal oscillations in rainfall extremes appear in a nearly cyclic manner with periods of 30 to 40 years (Figure 1). A period with only 3 cycles is too short to draw statistically strong conclusions on this property, but results clearly indicate the presence of long-term temporal persistence in the rainfall extremes, with a cluster of rainfall extremes during the past 15 years. These conclusions are consistent for all time scales varying from 10 minutes to the monthly scale, and both for the winter and the summer season (Figure 1). For the summer period, highest extreme rainfall quantiles are observed in the 1960s, slightly higher than the more recent ones from the past 15 years. These results suggest that the recent increase in the number of heavy showers causing sewerage system flooding, is caused by hydrometeorologic conditions which are less or equally extreme than what was observed during the 1960s. Of course, in the mean time, land use strongly changed (e.g. urban areas expanded and sewerage systems were built at a large scale) such that hydrological effects nowadays strongly differ from the ones in the 1960s.

For the winter period, observations are different. Extreme rainfall quantiles during the past 15 years are 25% higher in comparison with the 108 years average (Figure 1), which is 9% (for monthly rainfall volumes) to 19% (for 10 min rainfall intensities) higher than during previous cluster periods of the past century. Results show an increase in extreme rainfall quantiles for the winter period, but no clear increase for the summer season (however, summer extremes at larger time scales show a decreasing trend). The high perturbation factors in the 1910s-1920s, 1960s and 1990s and the low factors in the 1930s-1940s and 1970s are significant at the 5% significance level. They appear to be explained both by an increase/decrease in the number of extreme rainfall events and by a higher/lower rainfall intensity per event, although the former factor is most important.

The transitional seasons of autumn and spring showed different results (Figure 2). In contrast to the observations for winter and summer, there were no persistent clusters and trends for autumn. Spring, however, had some clustering periods with a few indications of increasing trends for the most recent decade similar to the winter trends although the cluster periods were limited. The 10 minutes time scale perturbations for spring had significant positive trends for the most recent decades. High rainfall extremes for the spring were mainly persistent in the 1980s at the daily and monthly time scales. It is notable that the clustering period for spring differs from the cluster periods in summer and winter.

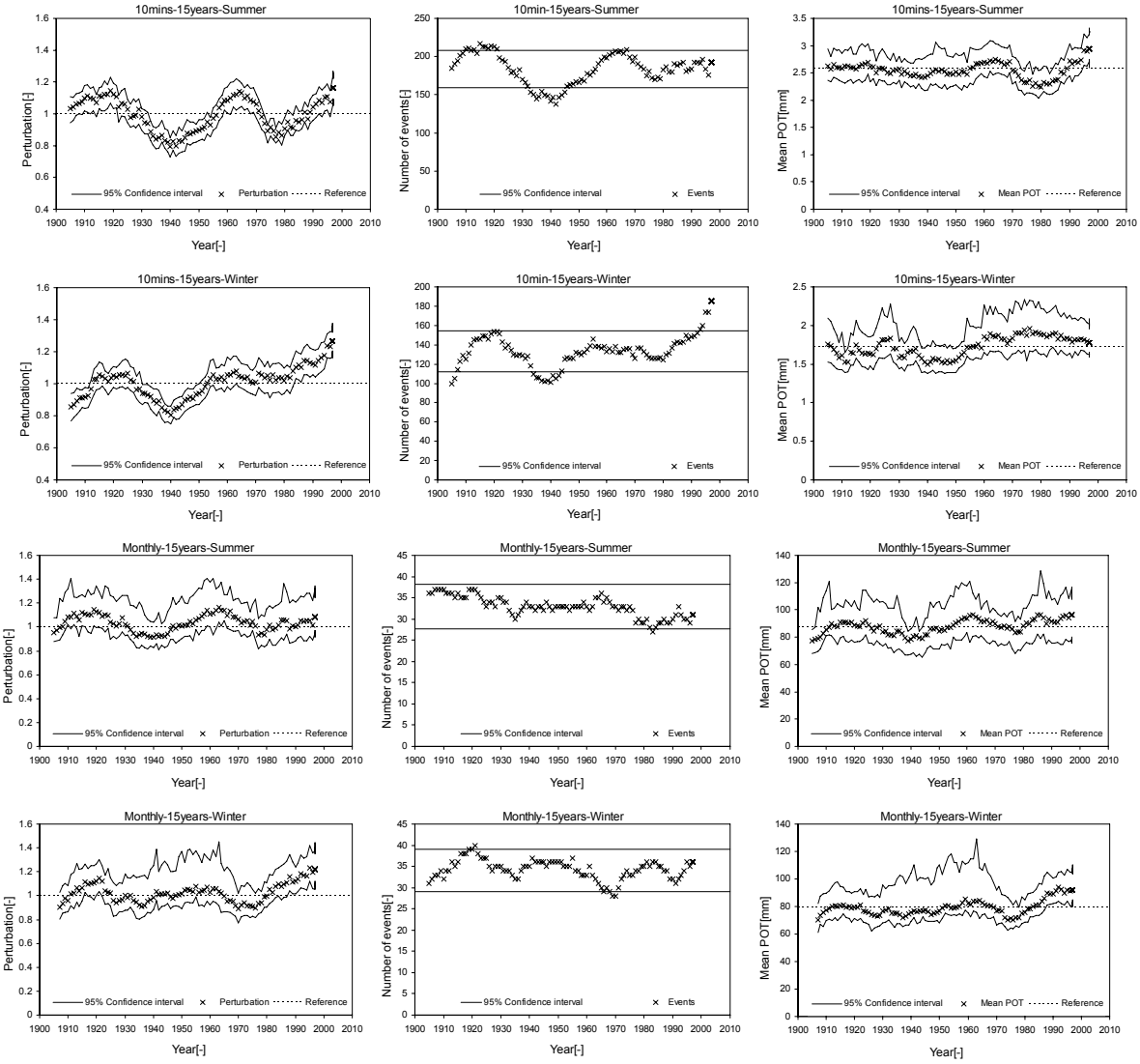

Figure 1: Estimates of average quantile perturbations, number of events and mean POT values for 10 minutes and monthly rainfall extremes, and 15-year blocks for summer and winter periods, together with 95% confidence intervals under the hypothesis of no persistence in trends and oscillations.

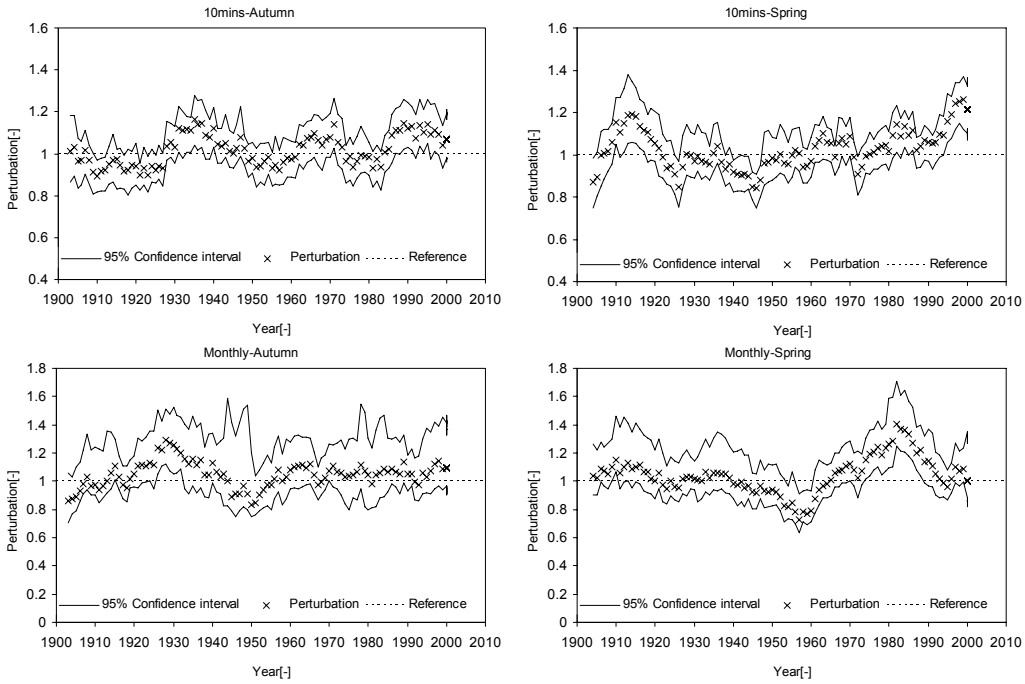

Figure 2: Estimates of average quantile perturbations for 10 minutes and monthly rainfall extremes, and 10-year blocks for autumn and spring periods, together with 95% confidence intervals under the hypothesis of no persistence in trends and oscillations.

3.4 Evapotranspiration historical trends

Evapotranspiration plays a key role in hydrological impact studies as it represents a loss of water from the hydrological system. It also provides a nexus in the hydrological cycle between the hydrosphere and the atmosphere. As a result, ETo changes are correlated with other climatological variables; thus, findings can be used to explain changes in other variables. Unlike precipitation which is highly variable, evapotranspiraion (ETo) is considered less sporadic. Therefore the analysis of ETo is somewhat less complicated.

Evapotranspiration has hitherto not been extensively studied for climate change studies partly due to its invariable seasonal nature, and the paucity of reliable long records of the various variables required for calculating potential evapotranspiration: wind speed, air pressure, humidity, temperature, and solar radiation. Also, ETo assessment is difficult, as direct measurements are usually expensive, and sophisticated. ETo studies have been simplified by approximate methods which provide reasonable estimates. For instance, approximate methods exist for estimating ETo primarily based on temperature differences but such methods tend to make spurious estimations especially in humid climates and thus require bias corrections. The climate of Western Europe is highly dependent on the atmospheric circulation. Wind speed is an important driving force for ETo. The Penmann-Monteith equation, which among other variables includes wind speed, is currently favoured for estimating evapotranspiration; but for more reliable results the parameters need to be calibrated. From a rigorous study, Bultot [1983] calibrated the Penman-Monteith equation for the local conditions in Belgium. The ETo trends were studied for a time series generated from this Bultot method.

A statistical trend analysis for evapotranspiration is important for climate change studies. An ETo trend analysis will reveal periods of increasing or decreasing trends which may be used to infer changes in climatic and hydrologic systems. For example, ETo and precipitation can be used for studying the dryness of periods. Coincident decreasing trends of ETo and increasing rainfall trends would signal a risk of floods. Conversely, increasing ETo trends and decreasing rainfall trends would trigger droughts and low flows. The trend analysis is also important for checking historical ETo trends with expected future trends from the climate models. Climate models may be assessed for suitability by checking if they reproduce the trends of the observed ETo. This, however, is still difficult due to the imperfectly modelled physics related to evapotranspiration. In particular, the physics in soil-water models present a conundrum for climate modellers.

Following a similar procedure for analyzing trends for precipitation, the Uccle ETo was examined. The ETo daily data was provided by IRM/KMI for the daily period 1901-2005. The quantile-perturbation technique was used for the analysis. This technique was previously used for the historical trend analysis of precipitation. The ETo anomalies were analysed solely based on the long term average perturbation (perturbation=1); for rainfall 95% confidence intervals were calculated but for ETo this was unrealistic as ETo data failed to fit the traditional distributions. The daily, weekly, and monthly time steps were studied. Notwithstanding the limitations, the quantile-perturbation technique provides insights in the variability of ETo trends especially regarding the temporal anomalies.

The seasonal perturbations were examined for all the climatological seasons: summer, autumn, winter, and spring. Like rainfall, the assessment was also based on reasonably high thresholds to eliminate the spurious perturbations from ETo rates close to zero. Figure 3 exhibits the perturbations for the four climatological seasons.

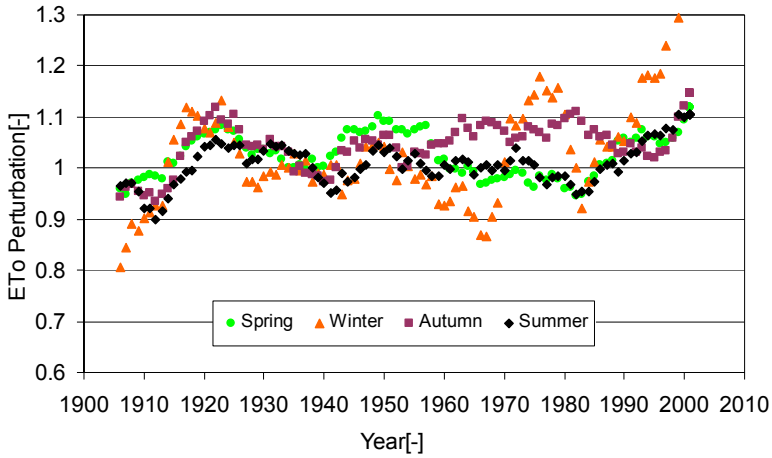

Figure 3: Estimates of average quantile ETo perturbations for monthly data covering the period 1901-2005 for summer, autumn, winter, and spring seasons.

The summer season did not show significant trends as most of the perturbations were fluctuating around the long term perturbation of 1. Typically, ETo is highest during summer but the relative changes indicate that on average ETo was fairly constant (before the 1990s). Maximum perturbations of about 10% were observed for the most recent decade. Overall the perturbations were 10% above and below the long-term average.

Autumn experienced slightly higher perturbations than summer and spring especially since the 1960s. A maximum of around 15% for the most recent decade was observed at the monthly time scale. The perturbations were ranging between -10% and 15%.

The winter season showed the most significant changes with the most recent decades appearing more pronounced. There have been some significantly high perturbations notably the 1970s and the most recent decade (1990s) showing the highest perturbations of up to 30%. The low perturbations were found in the 1960s and were 15% lower than the long term average.

The spring perturbations were similar to the summer perturbations albeit generally slightly higher. A maximum of 10% (1920s and 1950s) and a minimum of -5% were observed.

All in all, since the 1980s there have been increasing ETo trends especially during the most recent decade with winter showing the most pronounced changes. These changes are consistent with the current temperature trends which have shown warmer winters than previously recorded. Various studies have also indicated that the future winters will become milder which implies that ETo rates will increase further. This will increase the amount of water vapour in the atmosphere and therefore lead to an increased rainfall potential in winter.

4 Model performance

A model may be tested for its ability to reproduce the meteorological characteristics including mean statistics, seasonality, spatial variability, inter-annual variability, and trends. If a model performs poorly, it can either be rejected or given a low weight to reduce its impact on the overall uncertainty. Several performance tests were carried out at both a local scale (comparing with the Uccle series) and the regional scale (for the whole of Belgium).

4.1 Methods and tests used at local level

To examine the inconsistencies, the main tests entailed statistics of errors, biases, correlations and trends. The RCM data was statistically checked for inconsistencies by quantifying the differences between the models and the historical time series from RMI at Uccle. The mean temperature, maximum temperature, minimum temperature and rainfall were assessed. These variables play a very important role in hydrology and constitute the fundamental meteorological variables in general. The data was also checked for monthly, seasonal and annual differences.

The time series of the control simulations were compared with the corresponding time series of observations of the same physical quantity (temperature, rainfall). The monthly mean was computed for temperature while the total accumulated was computed for the rainfall values. From the new time series it was then possible to perform the tests. The number of control simulations was 21 for rainfall, 20 for mean daily temperature, and 19 for minimum and maximum temperature.

To test the mean error and bias of the frequency distributions of certain temperature and rainfall events, the events were grouped as follows:

- For rainfall, number of days per year with: more than 10 mm, 20 mm or 40 mm, or less than 0.1 mm of rainfall.
- For temperature, number of days per year with: minimum temperature below 0°C (freezing days), maximum temperature below 0°C (winter days), maximum temperature above 25°C (summer days), maximum temperature above 30°C (hot days).

The RCM time series were also assessed based on standard statistical tests to detect the existence of trends or change-points in the model simulations and in the reference historical time series from RMI at Uccle. From the original daily time series, annual time series were computed and the tests were applied. In particular, the Kendall coefficient, Pettit [Pettit, 1979], and Lombard tests [Lombard, 1988] were performed.

4.1.1 Error, bias

The error and bias for each model were computed against the Uccle series. A brief discussion of the computation follows. Let $\{(X_p)_i\}$ be the time series of the control simulation p, $p \in \{1,\ldots,M\}$, and let $\{Y_i\}$ be the corresponding time series of observations of the same physical quantity (temperature, rainfall). The mean error between the climatological values of the two time series is calculated as follows. From $(X_p)_i$ and Y_i two new time series are generated, $(X_p)^k$ and Y^k, $k \in \{1,\ldots,K\}$, with the monthly mean, for temperature, or total accumulated, for rainfall, values. From the new time series, the root mean square (RMS) error E_p and bias B_p are calculated as:

$$E_p = \sqrt{\frac{1}{K}\sum\left((X_p)^k - Y^k\right)^2}$$

$$B_p = \frac{1}{K}\sum\left((X_p)^k - Y^k\right), \quad p = 1,\ldots,M$$

The number M of control simulations is 21 for precipitation, 20 for mean daily temperature and 19 for minimum and maximum temperature. For the case of monthly means or accumulated totals, the number K has the value 12.

The percentage values were calculated as yearly means (for temperature) or yearly totals (for rainfall) and for some cases the climatological values were analysed. Figure 4 shows the error and bias plots for rainfall and temperature.

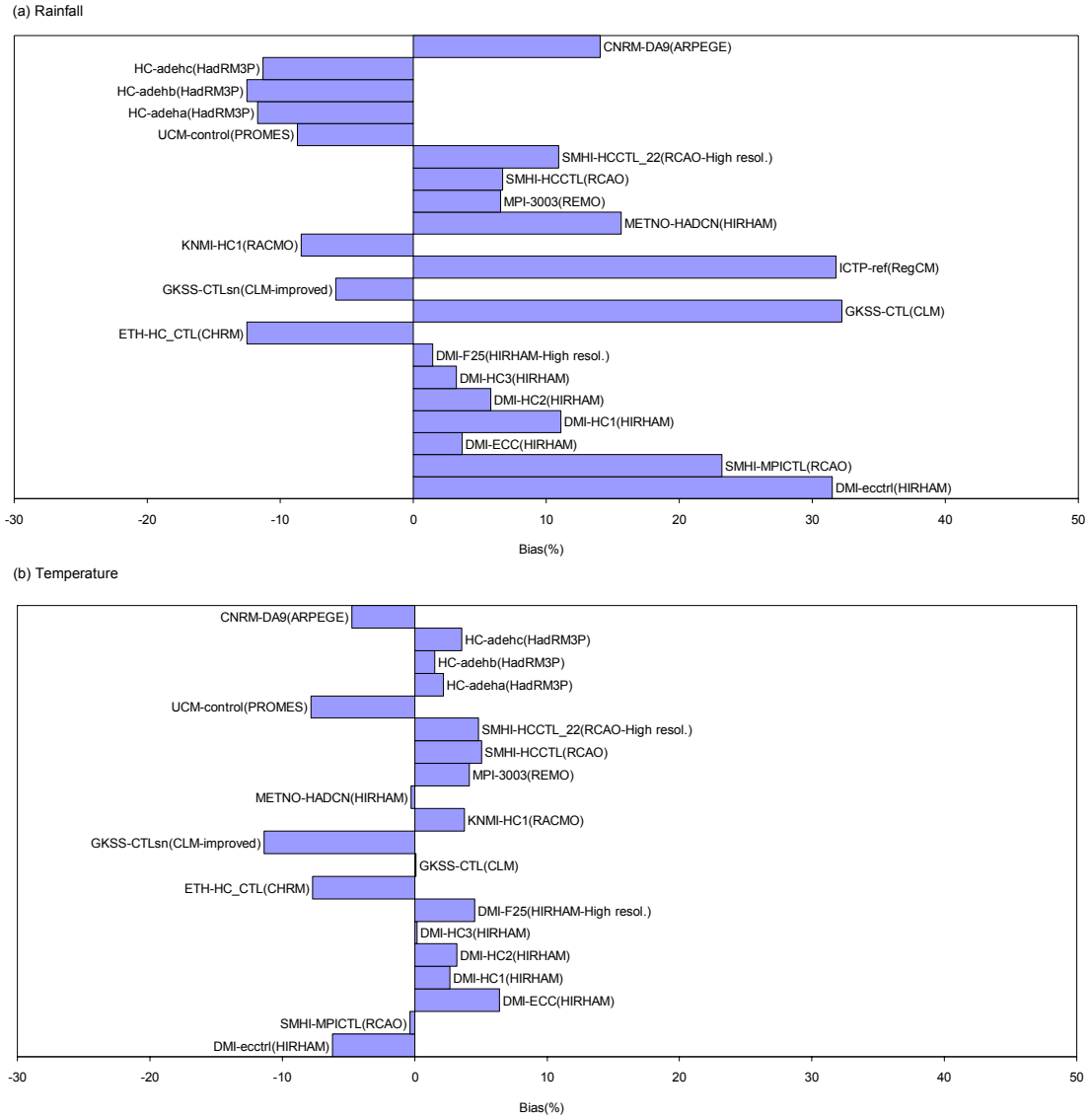

Figure 4: Bias for rainfall (a) and temperature (b) for the PRUDENCE climate models. The RCMs are indicated enclosed in brackets after the run codes.

For the assessed models the climatological profile of the temperature is simulated better than rainfall. The rainfall, being inherently less predictable, is less well captured in the simulations. It is interesting to observe that the higher-resolution simulations (at 25 km) do not necessarily perform better than the high-resolution simulations (at 50 km); generally the errors are lower in the higher resolutions (25 km), but there are some simulations at 50 km with even less error.

The bias for both rainfall and temperature alternates around zero with more wide variations for the rainfall. However, the overall mean bias per model simulation is not far away from zero: 6.04% for the rainfall and 3.54% for the temperature. So, based on an ensemble mean, the models have a small positively bias for both variables. The principle of ensemble modelling requires that the mean of all the model results is used instead of the individual models. This mean error analysis is a classic example of ensemble modelling. The ensemble mean performs better than most individual models.

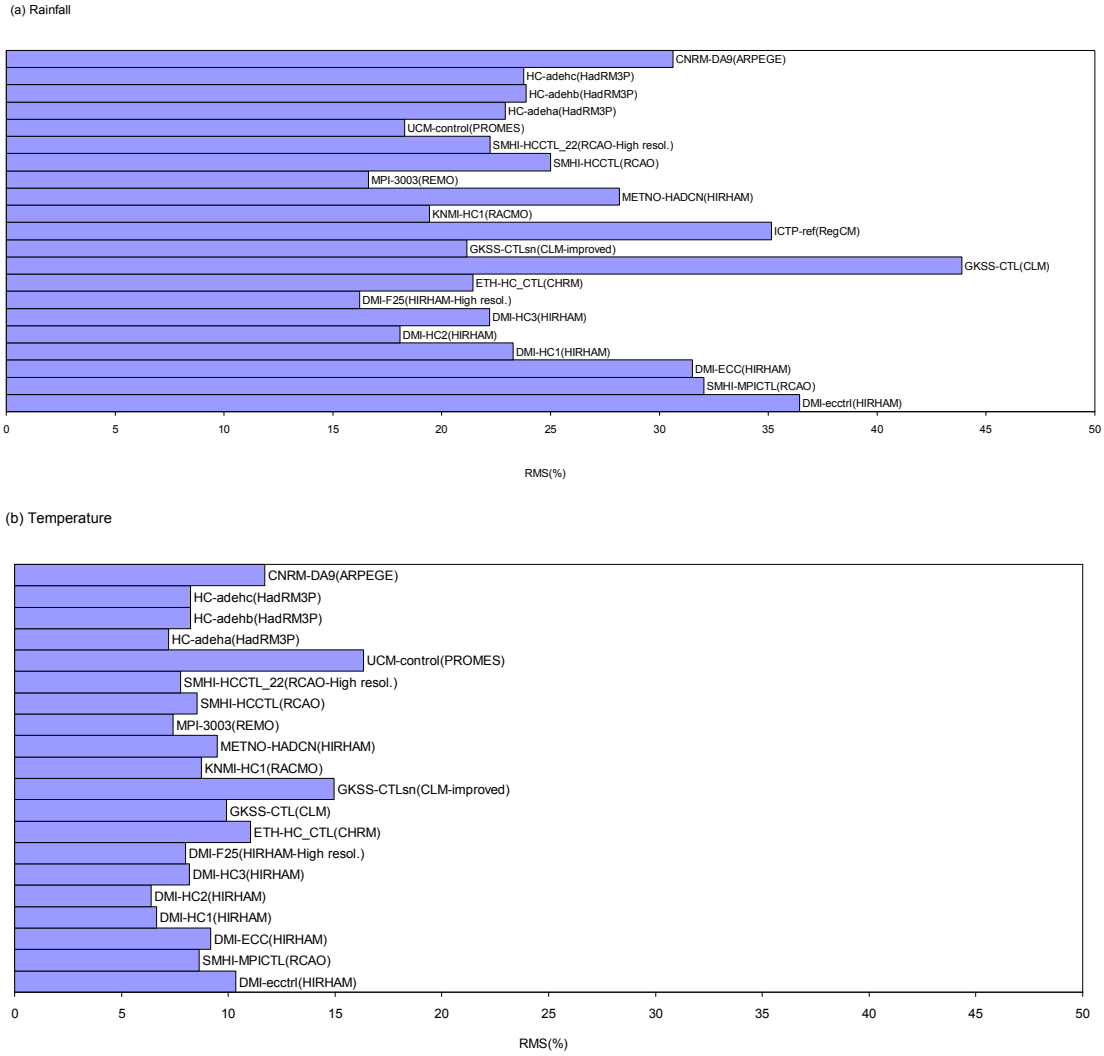

Figure 5: RMS error for rainfall (a) and temperature (b) for the PRUDENCE climate models. The RCMs are indicated enclosed in brackets after the run codes.

Inevitably, there are two separate classification schemes: according to rainfall and according to temperature. Considering the RMS error as a performance measure (Figure 5), CNRM-DA9, DMI-ECC, DMI-ecctrl, GKSS-CTL, ICTP-ref and SMHI-MPICTL appear to be in the upper half of errors for rainfall. It is notable that the simulations DMI-ECC, DMI-ecctrl, and SMHI-MPICTL have ECHAM model (version 4 and 5) as the driving GCMs. CNRM-DA9, GKSS-CTLsn and UCM-control were exceptionally anomalous for temperature.

The frequency bias for certain events of temperature and rainfall was also investigated. This involved a yearly summation of the number of events in both simulated and observed time series, and then the computation of the bias. A few thresholds were selected for the analysis. These events represent important thresholds for humid climates in general and for Belgium in particular. The temperature events were checked on a yearly basis while the rainfall events were studied based on the climatological winter (December-January-February) and climatological summer (June-July-August). Figure 6 shows the frequency bias for the selected thresholds. The threshold of 0mm represents the bias for days less than 0.1mm which are taken as dry days. For the other thresholds, the frequency bias represents the number of days above the thresholds.

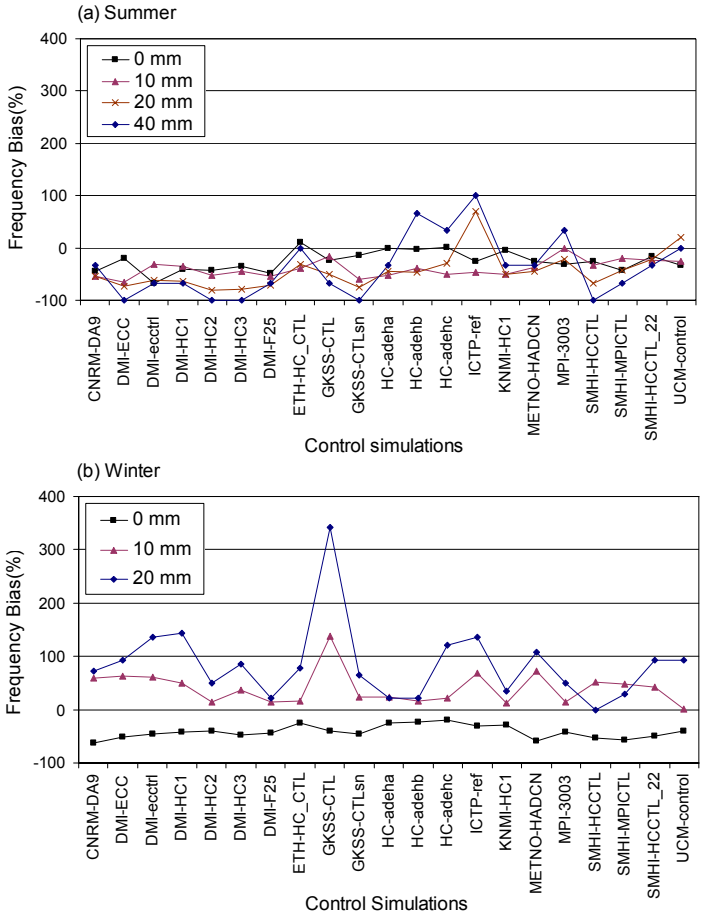

Figure 6: Rainfall frequency bias based on different thresholds for summer (a) and winter (b). The 40mm threshold has not been considered for winter, as there are no observations above 40mm.

It is evident from the behaviour from the frequency bias of the extreme events that all models have some difficulty of capturing the climatic behaviour of such events. There is a tendency for overestimation of the extreme events and an underestimation of the number of dry days during winter. The data for the 40 mm events in climatological winter have not been plotted since the normalized bias cannot be computed in this case (the number of observed events here is zero). During winter, the GKSS-CTL simulation overestimates more than the other models the 10, 20, and 40 mm events frequencies. During summer, however, there is a general negative frequency bias of events. Another notable exception is the case of the ICTP-ref simulation which is positively biased for events larger than 20mm. This observation is consistent for the two seasons.

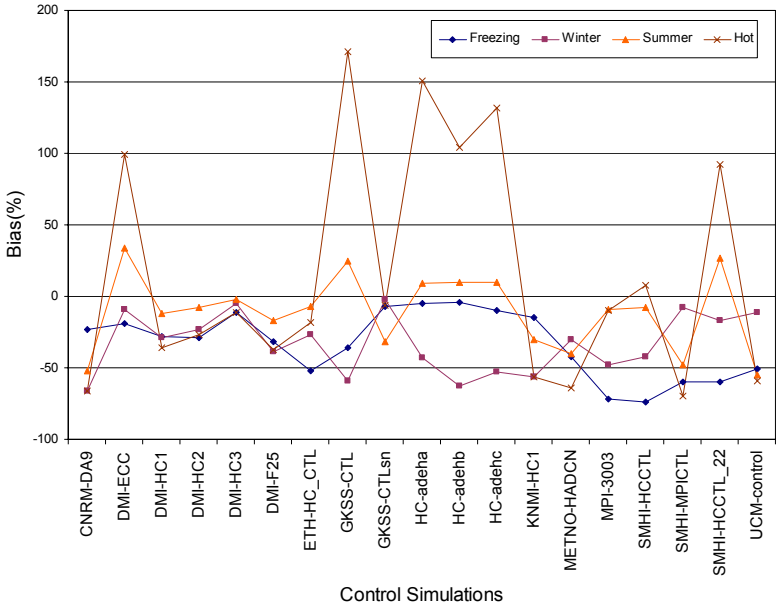

Figure 7: Temperature frequency bias based on different thresholds: the freezing days (minimum temperature < 0°C), winter days (maximum temperature > 0°C), summer days (maximum temperature > 25°C), and hot days (maximum temperature > 30°C).

For temperature (Figure 7), there is also a general underestimation of the frequency of the prescribed events (freezing, winter, summer and hot days) with the exceptional observation of the number of hot days. 6 simulations have large overestimations, which may counterbalance all the other simulations if an ensemble mean is used. The simulations with anomalously high frequencies of hot days are: DMI-ECC, GKSS-CTL, HC-adeha, HC-adehb, HC-adehc and SMHI-HCCTL_22.

In the case of the temperature events considered, the errors are generally increasing in the order freezing days → summer days → winter days → hot days. The relative error (RMS error) can be too high: from 30.60% up to 81.98% for the freezing days, and from 115.55% up to 287.50% for the hot days.

4.1.2 Trend tests

Generally, the model simulations capture well the absence of trend in the observed times series, for both rainfall and temperature. The Pettit and Mann Kendall tests do not contribute in a clear way in assessing model performance. However, the Lombard change-point test detected inconsistencies in the time series of some models. For rainfall, the DMI-HC3 and SMHI-MPICTL showed evidence of change points while the GKSS-CTL, GKSS-CTLsn and UCM-control models were identified for temperature.

The model performance is summarized in Table 4 and Table 5 regarding RMS error, thresholds (annual or seasonal), and possible trend or change points. Only six control series appear to be ideal (no apparent faults) for the Belgian climate. This would imply that the seven series (DMI-HC1, DMI-HC2, DMI-F25, KNMI, MPI, METNO and SMHI-HCCTL) simulate the present climate well and would provide the best estimates for climate change. These six models would make the best selection but having only six models would greatly reduce the number of models. Since it is not guaranteed that a climate model, which simulates well the present climate, would simulate well the future climate it is better to take a more cautious approach. There is a need of more models because the increased number of models can provide insights concerning climate model spatial and temporal variability, and uncertainty. Even so, the assessment so far has only been done at the point data level. The regional evaluation is also necessary for a complete assessment.

Table 4: Model performance for rainfall

MEMBER	CODE	RCM	RMS	THRESHOLD	TREND
CNRM	DA9	ARPEGE	•		
DMI	ECC	HIRHAM	•		
	ecctrl	HIRHAM	•		
	HC1	HIRHAM			
	HC2	HIRHAM			
	HC3	HIRHAM			•
	F25	HIRHAM (High resol.)			
ETH	HC_CTL	CHRM			•
GKSS	CTL	CLM	•	•	
	CTLsn	CLM (improved)			
HC	adeha	HadRM3P			
	adehb	HadRM3P			
	adehc	HadRM3P			
ICTP	ref	RegCM	•	•	
KNMI	HC1	RACMO			
METNO	HADCN	HIRHAM			
MPI	3003	REMO			
SMHI	HCCTL	RCAO			
	MPICTL	RCAO	•		•
	HCCTL_22	RCAO (High resol.)			
UCM	control	PROMES			

Table 5: Model performance for temperature

MEMBER	CODE	RCM	RMS	THRESHOLD	TREND
CNRM	DA9	ARPEGE	•		
DMI	ECC	HIRHAM		•	
	ecctrl	HIRHAM			
	HC1	HIRHAM			
	HC2	HIRHAM			
	HC3	HIRHAM			
	F25	HIRHAM (High resol.)			
ETH	HC_CTL	CHRM			
GKSS	CTL	CLM		•	•
	CTLsn	CLM (improved)	•		•
HC	adeha	HadRM3P		•	
	adehb	HadRM3P		•	
	adehc	HadRM3P		•	
ICTP	ref	RegCM			
KNMI	HC1	RACMO			
METNO	HADCN	HIRHAM			
MPI	3003	REMO			
SMHI	HCCTL	RCAO			
	MPICTL	RCAO			
	HCCTL_22	RCAO (High resol.)		•	
UCM	control	PROMES	•		•

4.1.3 Quantile/frequency analysis of rainfall

Climate models may satisfy mean statistics but fail to reproduce extreme distributions which are crucial for flood risk analysis. Through a quantile/frequency analysis, a model is evaluated for its ability to reproduce extremes. The ranked values of a control model series (1961-1990) are compared with the ranked values of the observed time series. The quantile analysis is expected to reflect the findings in the threshold frequency bias investigation. While the threshold analysis only focused on a few

thresholds, the frequency distribution check entails the entire set of observations leading to a better interpretation of the consistencies of the RCMs with the historical data. However, the quantile analysis should not be used solely for rejecting some model simulations. The frequency distribution check was applied for rainfall alone as temperature had previously been found to be less biased.

Figure 8 shows the frequency distributions for the winter and summer seasons respectively. During winter, the models approximate the extremes fairly well as the models are close to Uccle. The Areal Reduction Factor (ARF) of 0.8 was applied and also plotted to account for the expected systematic difference between the historical point rainfall at Uccle and the grid averaged RCM rainfall. The ARF introduces a spatial downscaling element as it converts the point data to a grid estimate. During summer, there is a general underestimation of extremes as many models are below the Uccle summer distribution. This analysis is considered a graphical approach as it allows easy spotting of discordant models. For a robust evaluation, the extreme statistics are complemented with statistical tests. With the aid of graphical and statistical techniques, GCMs and RCMs with significant biases can be spotted and better selections made to reduce the errors in projections. In terms of the frequency distribution, winter is better simulated than summer. The previous bias assessment based on number of events also revealed that the rainfall bias is negative in summer and positive in winter. Moreover, the same models appear anomalous: the CNRM for summer and GKSS for winter.

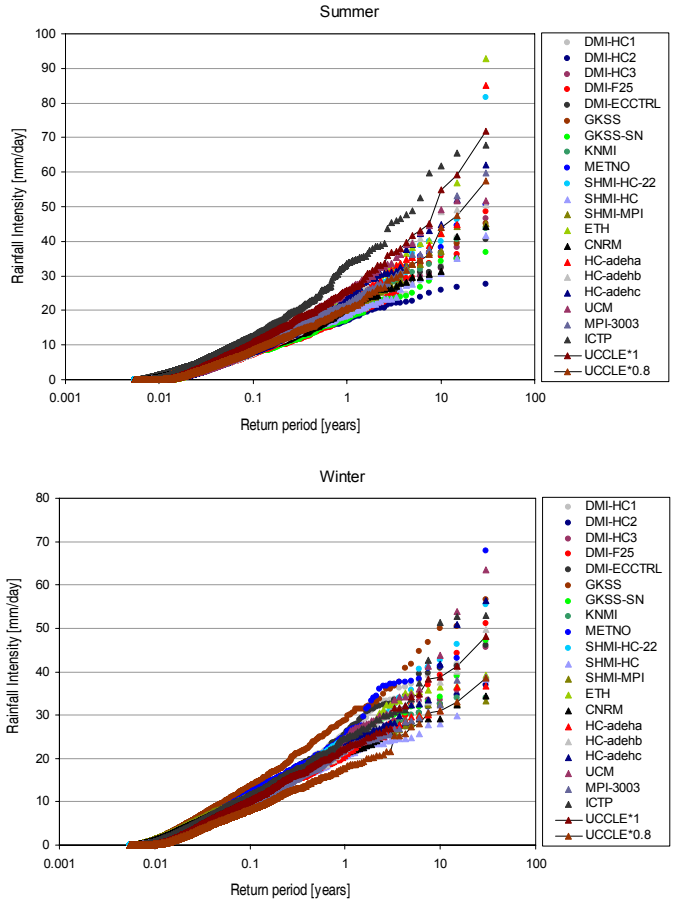

Figure 8: Frequency distributions for summer (top) and winter (bottom). The observed Uccle series are also plotted. An ARF of 0.8 was applied (Uccle*0.8) to account for areal differences between model grids and point observed data.

4.2 Model performance at regional level

Regional consistency of the models is also important as it can be used to reinforce the argument for rejection in addition to point evaluation. It would be realistic to discard models that are highly biased both locally and spatially. Spatial checks also implicitly detect differences in regional climates; climate models may simulate higher or lower meteorological variables in some regions compared to others. The regional performance was checked for rainfall only. The point rainfall model performance provides

an initial set of potential outlier models, which can now be checked regionally over Belgium. Similar concepts of bias and RMS error used earlier for point data are used with an extra dimension of a new areal performance measure, the covariance difference. The analysis is briefly explained next.

Let p_{ijk} be the mean rainfall over the control period for the model simulation i, month j and grid box k. Let accordingly p_{obs_jk} be the observed rainfall for the month j obtained by integration over the grid box k. The bias of the simulation i over the grid box k is defined by means of the formula:

$$B_{ik}=\frac{1}{12}\sum_{j=1}^{12}\left(p_{ijk}-p_{obs\_jk}\right)$$

Similarly, the RMS (Root Mean Square) error of the simulation i over the grid box k is defined as:

$$RMS_{ik}=\sqrt{\frac{1}{12}\sum_{j=1}^{12}\left(p_{ijk}-p_{obs\_jk}\right)^2}$$

From these equations one can calculate the areal mean values B_i and RMS_i of the bias and RMS error as an average of all the grid box values B_{ik} and RMS_{ik} respectively. These quantities depend only on the simulation i.

The covariance difference is a measure of simulation performance that has no analog in comparisons between point data (for example between one station and one grid point, as in previous calculations with the Uccle data). Using the rainfall variables X_{ijk} and X_{obs_jk} from the original time series (so that the index j runs now over the whole length N of the time series and not just over the months of the year as in the case of mean values), we can calculate the covariance matrices $C_i=\left(\mathrm{cov}(X_{ik},X_{il})\right)$ and $C_{obs}=\left(\mathrm{cov}(X_{obs\_k},X_{obs\_l})\right)$, where:

$$\mathrm{cov}(X_{ik},X_{il})=\frac{1}{N}\sum_{j=1}^{N}X_{ijk}X_{ijl}-\left(\frac{1}{N}\sum_{j=1}^{N}X_{ijk}\right)\left(\frac{1}{N}\sum_{j=1}^{N}X_{ijl}\right).$$

A similar equation defines $\mathrm{cov}(X_{obs\_k},X_{obs\_l})$.

One can then consider as the covariance difference the Frobenius norm of the difference between the two covariance matrices:

$$\left|\Delta C\right|_i^2=\sum_{k,l}\left[\left(C_i-C_{obs}\right)_{kl}\right]^2$$

This quantity captures in one number the difference of the statistical spatial dependences between the simulation i and the observations obtained by integrating the rainfall measurements over the grid boxes of the corresponding climate model.

The results of the calculations based on the previous regional analysis context (bias, RMS error and covariance difference) are presented in Figure 9 and Figure 10**.**

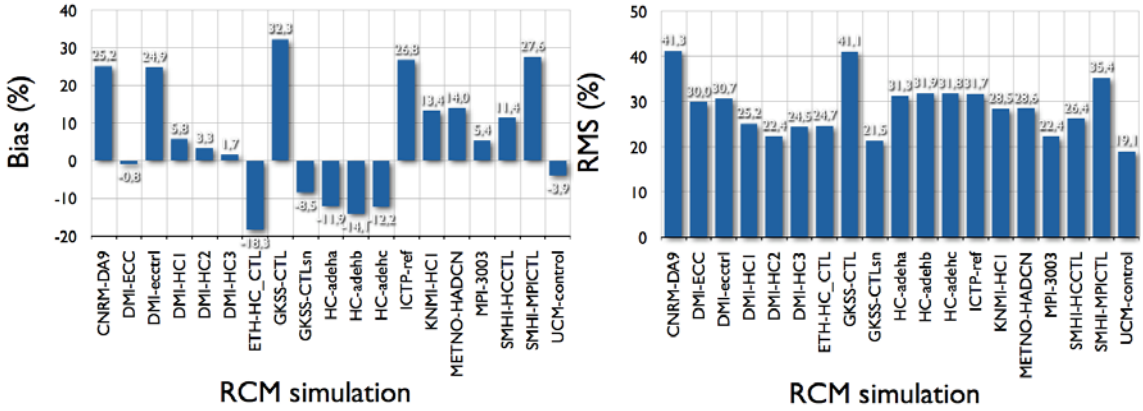

Figure 9: Average bias (left) and RMS error (right) for all control simulations.

The averaged bias over Belgium can be quite variable ranging about from -18% up to 32%. We readily distinguish three highly biased simulations, GKSS-CTL, ICTP-ref and SMHI-MPICTL, closely followed by CNRM-DA9 and DMI-ecctrl. The rest of the control simulations have biases less than 20% in absolute value. The average over Belgium bias picture presented in Figure 9 is not very different from the point assessment (Table 4 and Table 5) using the Uccle data as reference). For example, the change from the strongly negatively biased ETH-HC_CTL simulation to the strongly positively biased GKSS-CTL is still evident. Also, the three ensemble HC simulations are still negatively biased and by about the same amount. However, the KNMI simulation, which was negatively biased at on point (station-based comparisons), is positively biased over Belgium.

Figure 9 exhibits the averaged (over Belgium) RMS error for all control simulations. While almost all simulations exceed 20% of RMS error and some of them even exceed 30%, there are three that reach prominently higher values than the rest: CNRM-DA9, GKSS-CTL, SMHI-MPICTL, followed by the three ensemble HC simulations (adeha, adehb, and adehc) and ICTP-ref. From those, GKSS-CTL and ICTP-ref are also highly biased as detected previously. However, the area-averaged RMS error generally increases compared to the station-based (Uccle) estimations, with the most significant increase observed in the CNRM-DA9 simulation. Significant error increases are also observed in the three ensemble HC simulations. The changes in the other simulations are less important.

Figure 10 shows the covariance index (the covariance difference in %) for the control simulations. The model behaviour now can be radically different than in bias or RMS error. Perhaps the most representative examples are the cases of the CNRM-DA9 and SMHI-MPICTL simulations. Indeed, although these two simulations have fairly large RMS error, they show substantial performance improvement in the correlation test. On the other hand, there are two simulations that perform very poorly compared to the rest, exhibiting large deviations from the observed correlations: GKSS-CTL and ICTP-ref.

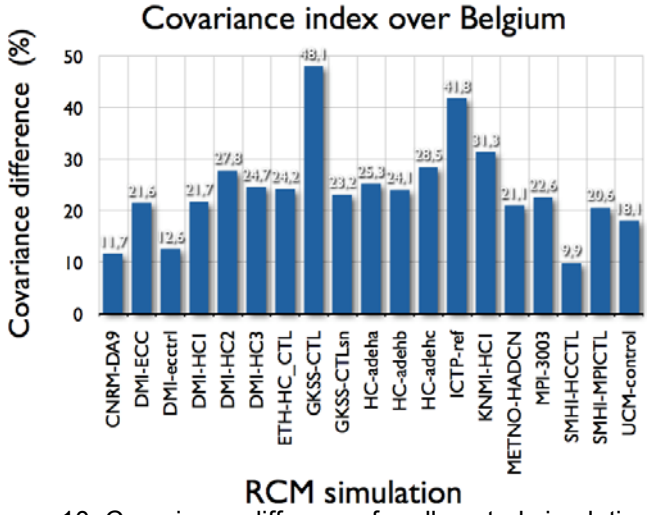

Figure 10: Covariance difference for all control simulations.

In summary, for the three spatial performance tests investigated for the control simulations of the models (bias, RMS error and correlation), two simulations showed consistently poor performance on every test: GKSS-CTL and ICTP-ref. Consequently, it is recommended not to take them into account in any subsequent analysis in the next phase of the project.

4.3 Selected climate models

The selection of the climate models is an amalgam of several criteria. By observing the behaviour of the control and scenario series using various statistics, some models were found to consistently perform poorly. It is notable, that no model performed well for all the criteria but some models were generally better than others. The outlier tests, frequency analysis, trend tests, bias measures, and spatial variability were the main criteria used for the climate model evaluation.

Table 6 shows the final list of the selected models. The ICTP (RegCM) and the GKSS (CLM) models were omitted from the list due to consistent discordant tendencies.

Table 6: Selected models and their respective GCMs and RCMs.

CONTROL	SCENARIO	SCENARIO	GCM	PRUDENCE RCM
SMHI	SMHI-MPI-A2	A2	ECHAM4/OPYC	RCAO
	SMHI-MPI-B2	B2	ECHAM4/OPYC	
	SMHI-HC-22	A2	HadAM3H	
	SMHI-A2	A2	HadAM3H	
	SMHI-B2	B2	HadAM3H	
KNMI	KNMI	A2	HadAM3H	RACMO
METNO	METNO-A2	A2	HadAM3H	HIRHAM
	METNO-B2	B2	HadAM3H	
DMI	DMI-S25	A2	HadAM3H	HIRHAM
	DMI-ecsc-A2	A2	ECHAM4/OPYC	
	DMI-ecsc-B2	B2	ECHAM4/OPYC	
	DMI-HS1	A2	HadAM3H	
	DMI-HS2	A2	HadAM3H	
	DMI-HS3	A2	HadAM3H	
ETH	ETH	A2	HadAM3H	CHRM
HC	HC-adhfa	A2	HadAM3P	HadRM3P
	HC-adhfe	A2	HadAM3P	
	HC-adhff	A2	HadAM3P	
	HC-adhfd-B2	B2	HadAM3P	
MPI	MPI-3005	A2	HadAM3H	REMO
	MPI-3006	A2	HadAM3H	
CNRM	CNRM-DC9	A2	ARPEGE	ARPEGE
	CNRM-DE5	A2	ARPEGE	
	CNRM-DE6	A2	ARPEGE	
	CNRM-DE7	A2	ARPEGE	
GKSS	GKSS-SN	A2	HadAM3H	CLM
UCM	UCM-A2	A2	HadAM3H	PROMES
	UCM-B2	B2	HadAM3H	

5 Climate change estimations

5.1 Overview of downscaling approach

Having identified the realistic models, the projections can now be determined by comparing the control simulations (1961-1990) with their respective future simulations (2071-2100). The projections were estimated based on frequency analysis of quantiles. The perturbation factors (ratio of the value in the scenario period versus the control period) are calculated for each empirical quantile (each empirical return period, or for the values with the same rank number after sorting). The perturbation factors are then plotted against the return period and the dependency of the perturbation factor on the return period investigated. For the higher return periods (more extreme conditions; typically for return periods higher than 0.1 years), mean perturbation factors are calculated for aggregation levels of 1 day, 1 week, 1 month, winter, and summer season. In Figure 11 the control and scenario rainfall quantiles are plotted for the winter and summer seasons. During winter, the scenario quantiles are above the control quantiles for the extremes, which implies that the intensity for a given return period increased; but for a given intensity, the return period decreased. Therefore, during winter, the future will experience an increase in frequency (reduced recurrence intervals) and an increase in intensity of the extremes. Summer presents an opposite response with a reduction in frequency (increased recurrence intervals) and a reduction in intensity. The patterns shown in Figure 11 are only for one model; other models may show a mixture of results with the scenario and control curves exchanging positions for different ranges of return periods. Figure 11c shows the perturbation factor which combines the frequency and intensity properties. A positive perturbation means that there is an increase in intensity and/or frequency while a negative factor implies a decrease in intensity and/or frequency. This explains the positive winter perturbations and the negative (perturbation<1) perturbations for summer. Also, the sharp bend shown during summer demonstrates the importance of a threshold. By selecting a 0.1 year threshold, the influence of the sharp bend is eliminated. This bend is somewhat linked to the positive feed backs within the climate models which lead to excessive drying of the soils in the soil-water models.

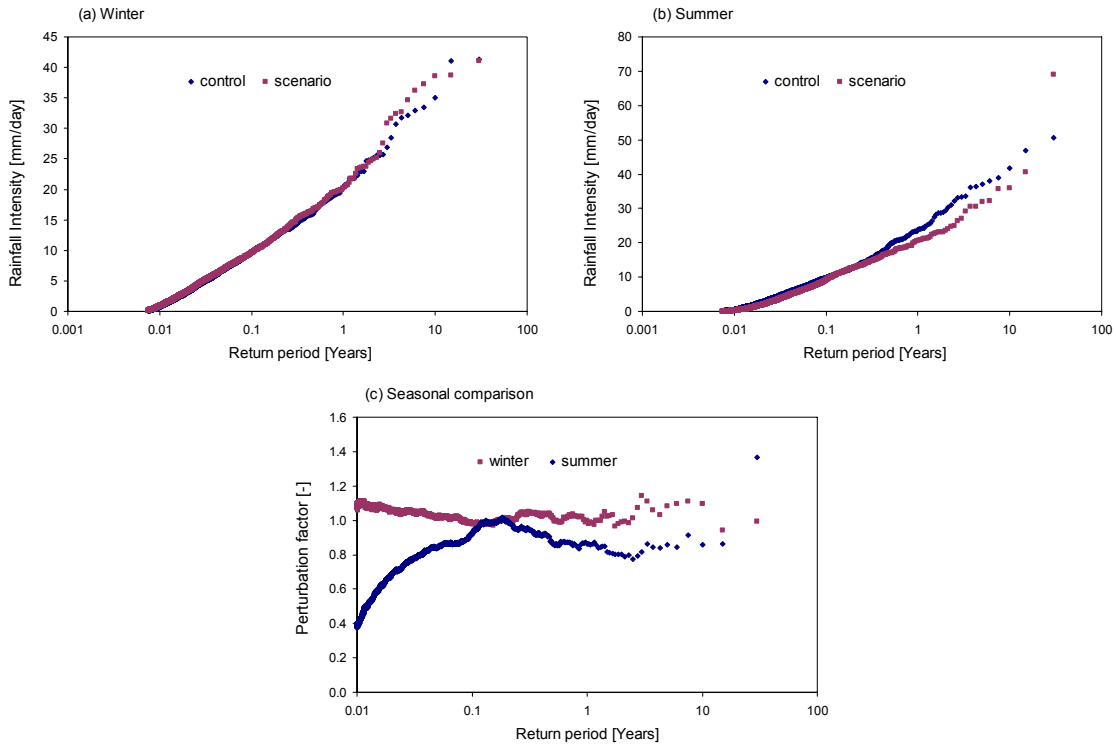

Figure 11: Rainfall distributions for winter (a) and summer (b), and the corresponding perturbations (c). The control (1961-1990) and scenario (2071-2100) series are shown for only one RCM to illustrate the typical perturbation patterns during the two seasons.

The quantile-perturbation analysis for the different aggregations was aimed at understanding the temporal variability of the perturbations. By definition, aggregations require the summation of values which implies a volumetric summation of rainfall quantities. By studying how the perturbations vary with aggregations it is possible to distinguish the internal variability of the base time series (the daily time step). Aggregation at different time scales implies a daily accumulation of quantities. By separating the daily values in seasonal time series, volumes for winter and summer were estimated at daily, weekly, monthly and seasonal scales. This was done for the control and scenario series after which the frequency perturbation technique was applied and an average perturbation calculated for values with recurrence intervals greater than 0.1 years. This was repeated for all the models for the rainfall and ETo series. The perturbation patterns across the different time scales revealed distinct seasonal behaviour.

From the perturbations three scenarios were identified to represent the highest, mean and lowest perturbations. It is apparent from Figure 12 that the rainfall changes are somewhat invariable for a given scenario during the winter season. This suggests that the number of wet days during winter does not significantly change. The perturbations during summer are generally lower than 1 (for the mean and low scenario) indicating that during summer all models predict reductions in perturbations. However, the reductions are highest during the seasonal aggregation. This suggests that by aggregating to seasonal scale the perturbations reduce mainly due to a reduction in seasonal volumes. This reduction in perturbations is perhaps explained by both the reduction in number of wet days and general reduction of intensity. The former factor appears to be more important as summer extremes were found to have increased and not decreased. Even so, the extremes make up a small percentage of the total number of wet days. The reduction in volumes can mainly be explained by an aggregation which includes the less extreme events hence leading to lower volumes. It follows that during summer, the reduction of wet days is important for climate change. The changes at different aggregations point to important characteristics which are relevant for downscaling which include the changes in both the number of wet days (for rainfall) and the intensities.

The perturbations for ETo have somewhat dissimilar features (Figure 12). The seasonal volumes tend to increase (with perturbations above one) for both winter and summer. The increase may be linked to the positive temperature perturbations in both seasons. The increase is more important during winter as there appears to be a significant increase from the monthly timescale to the seasonal timescale. This indicates that ETo changes are larger during winter due to the possibly higher temperature changes which can be inferred from the increased number of warm days. The higher temperature changes lead to higher ETo changes during winter. Whether the ETo changes will have a significant impact on the hydrological system will depend on the sensitivity of impacts to ETo. Floods tend to be less determined by the ETo changes but low flows are considerably affected by ETo.

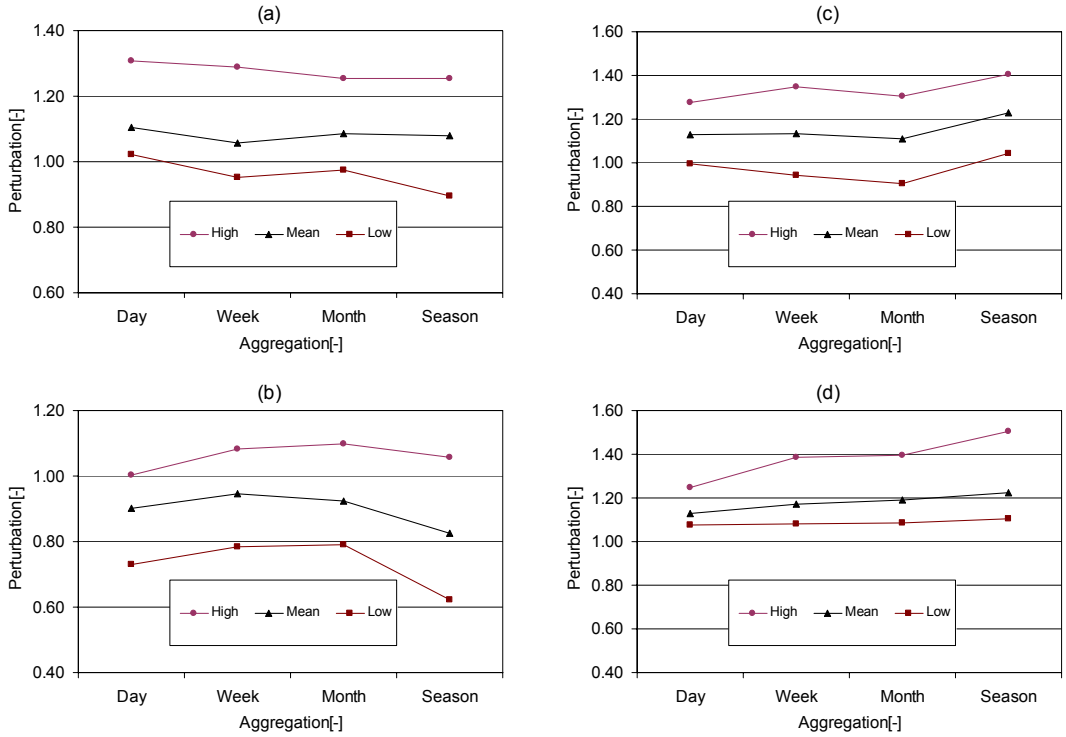

Figure 12: High, mean, and low perturbation factors for the different aggregations for rainfall in winter and summer (a and b) and ETo in winter and summer (c and d).

5.2 Projected climate change

The projections can now be determined from the control and the scenario series. It is important to note that the PRUDENCE RCMs were only based on the regional A2 and B2 scenarios and the projected outcomes should be interpreted as such. The number of models also leads to a range of expected changes which are a manifestation of the differences in the modelling physics of the models. Thus, a high, mean, and average projection can be provided for any future expected change. To understand the differences within the model projections, graphical interpretations are essential. With the models superimposed on the same graph systematic differences were spotted. The projected changes were first analyzed at a local scale (region close to Uccle) and then spatially (for the entire Belgium). Figure 13 shows the rainfall perturbations, which were derived as ratios of future seasonal volumes to present seasonal volumes. The discordant models identified previously (from ICTP and GKSS) have been deliberately included to highlight a remarkable observation: despite the biases, and model physics differences, the model projections are closer to each other. The outlier lines were determined using the extreme outlier boundaries of the box-and-whiskers plot [Tukey, 1977]. The similar climate projections may be explained by the fact that the models have similar boundary GCMs. Indeed, most of the models have the ECHAM4/OPYC3 and HadCM3 as boundary GCMs which were found to have similar global climate change (IPCC, 2001). However, the PRUDENCE set of models remains unique for its regional focus and thus the projected changes would be a first realistic case for future regional changes. The local changes (Figure 13) generally predict an increase of rainfall during winter (perturbation>1) and a decrease in rainfall during summer (perturbation<1). The winter seasonal changes are in the range of -10% to +26% while the summer changes are in the range of -40% to +6%. Other interpretations may also be made from the graphical plots. For instance, models may be categorized as high, mean and low. Differences in scenario projections may be quantified although for the seasonal case the A2 and B2 scenarios showed similar signals. The effects of the resolutions can also be inferred from the plots.

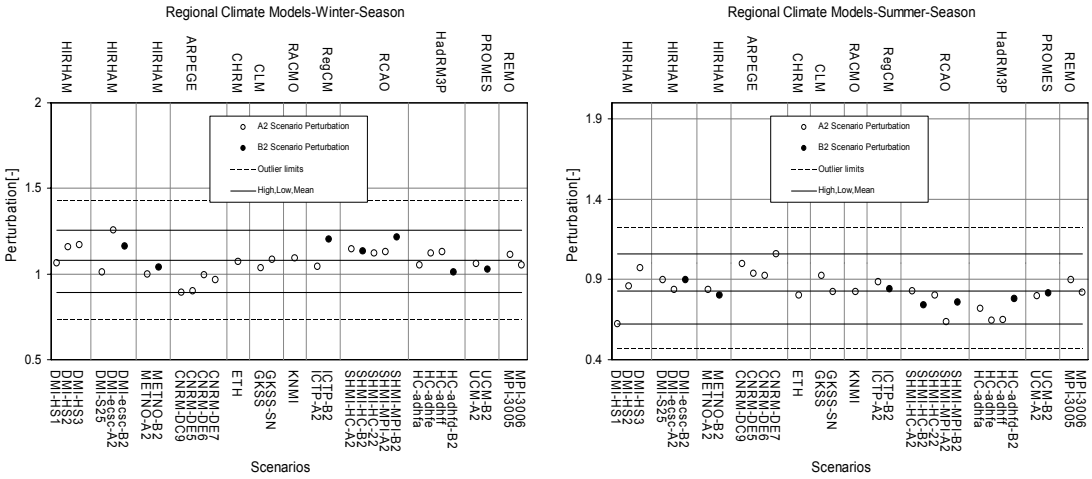

Figure 13: Local rainfall projections for winter (left) and summer (right). Dotted lines show the outlier limits (there are no outliers). The range of projections is defined by the high, mean and low factors.

5.3 Trend consistency check for the PRUDENCE RCMs

The historical trend analysis is also useful in checking RCMs for consistency with the historical climate. It would have been ideal to rerun the climate models for longer periods to check whether the models reproduce the observed trends and oscillations. However, this is impractical as it has implications for the calculation times considering the number of models involved. Thus, a different approach was to check whether the projected changes are realistic in retrospect. This requires extrapolating backwards in time. For a comparison with the model projections to be valid, the historical perturbations were recalculated for 30 year block sizes; RCM experiments are run for 30 year periods. The new trends and oscillations were compared to the future projections. Since the perturbations had a cyclic component, the perturbations were first de-oscillated such that only the trends would be compared. It is important to keep in mind that comparisons with the historical perturbations are only possible after 1961 which is the beginning period of the control simulations.

Based on the quantile-perturbation technique, the historical perturbations are recalculated for 30-year blocks for the period 1898-2005. As explained earlier, the points are plotted centrally within each block. After plotting the points, Fourier analysis is applied to fit cyclic patterns to the perturbations. The cyclic component is then subtracted from the total perturbation to eliminate the oscillation component from the time series leaving only the trend component.

With the quantile-perturbation approach average extreme perturbations are calculated for the RCMs by comparing the 30 year control series (1961-1990) with the 30 year scenario series (2071-2100). The perturbations calculation here depends on two series which is not the case for the historical series where the perturbations are based entirely on the historical series. Calculating the average perturbations for the period 2071-2100 for all the models leads to a range of factors. These factors represent the average increase or decrease in the extremes relative to the control period (1961-1990). By plotting a line joining the 1975 (centre of 1961-1990) and the factor at 2085 (centre of 2071-2100), a trend is traced. Instead of tracing all the trends for all the models, only the extreme trends have been shown in Figure 14. The perturbation represents a change relative to the baseline 1961-1990, which thus has a perturbation of 1. The analysis was repeated for both winter and summer. For both seasons, the historical trends are consistent with the global warming impact predictions by regional climate models; the historical trends are enveloped by the range of future projections. Therefore, in retrospect, the projected changes from the climate models are credible.

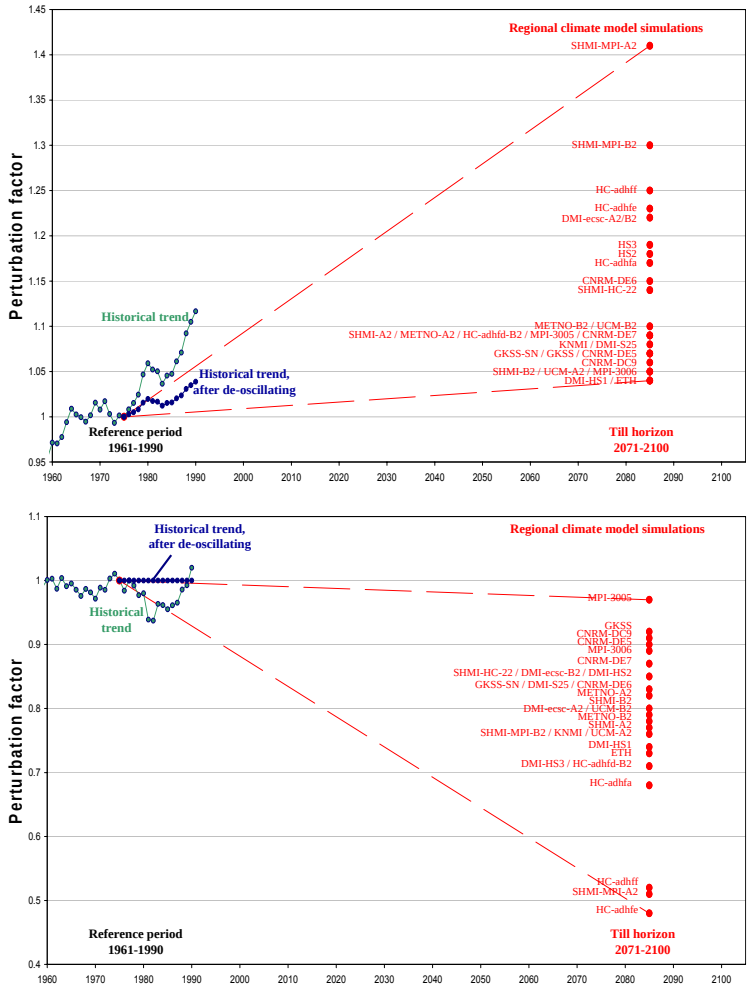

Figure 14: Comparison of the recent historical trends of daily rainfall extremes at Uccle for 30 years block size (from 1961-1990 till 1976-2005), before and after elimination of the approximate cyclic multidecadal oscillation contribution, with PRUDENCE RCM simulation results from the reference period 1961-1990 till 2071-2100, for winter (top) and summer (bottom) season.

5.4 Regional climate projections

The climate change projections from the PRUDENCE RCM simulations were also derived at the regional level over Belgium. Model performance was assessed spatially by taking into account model grid boxes with at least 70% lying within Belgium, where the observed precipitation has been integrated. The climate changes were calculated by comparing the control with the scenario RCM simulations. The results were rather heterogeneous making the interpretation of the climate change difficult. For example, in Figure 15, the climate change projections from the PRUDENCE member CNRM (Météo France) for the hydrological summer and winter seasons are displayed. The results are presented in the form of maps of Belgium with the corresponding grid boxes colored by shades of grey. Darker shades correspond to higher algebraic values, that is, higher absolute values whenever positive and lower absolute values whenever negative. The physical quantity represented is the precipitation change expressed as a percentage.

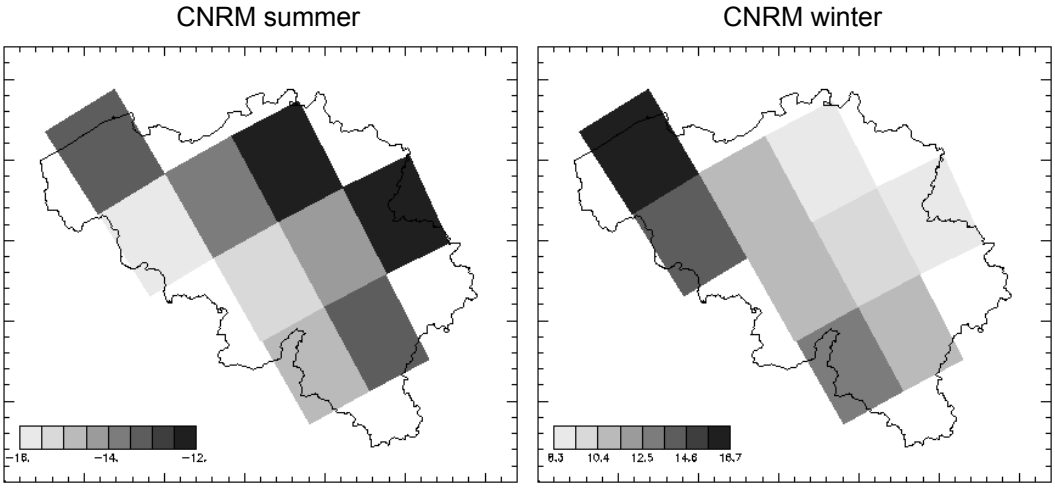

Figure 15: Rainfall climate change under SRES A2 scenario conditions for the CNRM climate model.

The summer map exhibits negative changes in rainfall, while the winter map exhibits positive changes. The RCM perturbation factors calculated locally (Figure 13), also agree with this rainfall change regime. Although these maps represent a certain climate change signal, there are two difficulties: (1) it is not very clear in which way the whole country is affected; (2) the climate change pattern can be quite different for another combination of control/scenario simulation from the PRUDENCE database. For this reason, the data from all simulations were projected to a common grid with much higher resolution (7 km x 7 km) and we proceeded to studying the data collected over each small grid cell. This allowed for a synthesis of all RCM data from the PRUDENCE database and provided a clearer picture of the projected climate change over Belgium.

The low, mean, and high perturbation factors were defined for the new and finer grid from the selected scenarios over a region including the Belgian territory. The six maps in Figure 16 and Figure 17 display the results for the hydrological summer and winter. There were no significant regional differences in the climate change signals over most of Belgium.

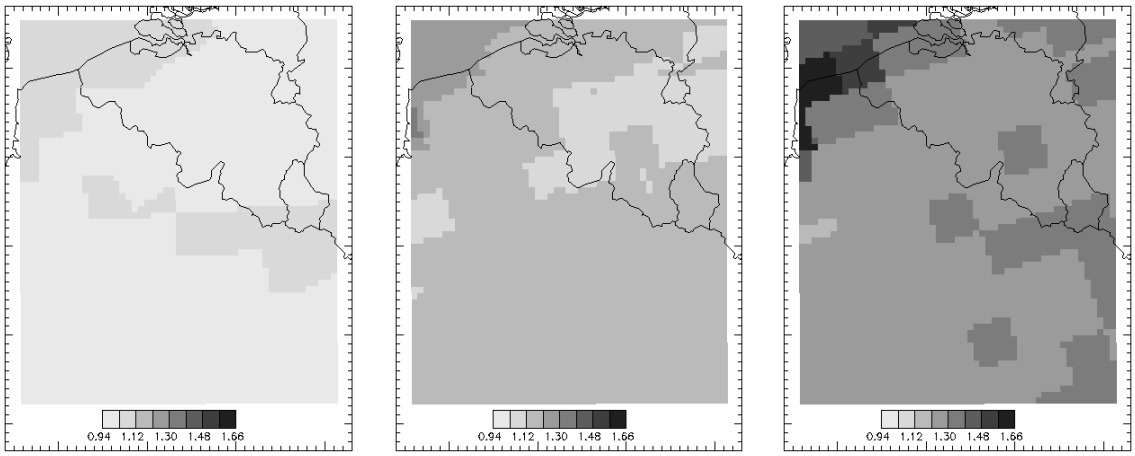

Figure 16: Low (left), mean (middle) and high (right) perturbation factors for precipitation over Belgium in the hydrological winter.

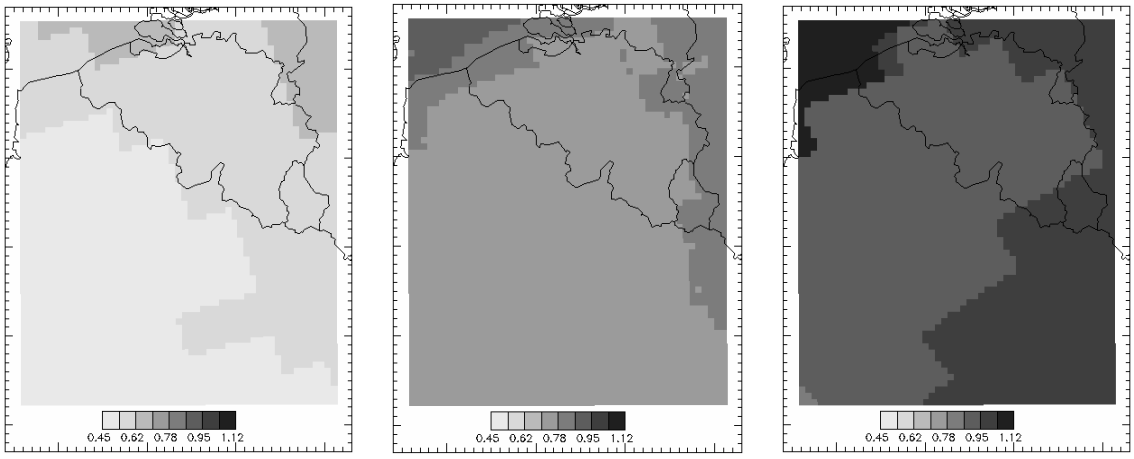

Figure 17: Low (left), mean (middle) and high (right) perturbation factors for precipitation over Belgium in the hydrological summer.

Despite the presence of some rather random fluctuations, especially in winter, some regional differences are discernable. The coastal area (north-north west) was identified as the geographical zone where the perturbation factors are systematically higher than in the rest of the country. This means that along the coast the precipitation increase in winter is expected to be more important, and that the precipitation decrease in summer is expected to be less strong, or even non-existent if the high scenario occurs. The difference in the perturbation factors between the main and coastal Belgium is of the order of –15% for all the seasons. The expected range of changes in rainfall during summer is -40% to +10% while the range in winter is +50% to +5%. The rainfall increase is expected to be more important in parts of the coast (north-northwest Belgium) and probably in the Ardennes region (extreme southeast).

6 Climate change downscaling

After evaluating the available RCMs and understanding the inconsistencies therein, the analysis progressed to statistical downscaling. Statistical downscaling (SD) ensures that the now realistic projections from the RCMs are transferred to the local observations. Conventional SD techniques require the use of statistical relationships obtained by comparing synoptic scale variables (predictors) with meso scale regional variables (predictands). These techniques, however, tend to focus on mean tendencies and overlook the changes in extremes which are essential for impact analysis. The PRUDENCE project primarily set out to use dynamic downscaling for fine scales to better represent the regional climate in Europe. Nonetheless, the RCM evaluation revealed biases despite the dynamic downscaling methods employed from the various models. Thus, the RCM results could not be used directly; hence the downscaling methodology required further modifications particularly those relating to changes in extremes. In essence, the dynamically downscaled results required statistical downscaling.

The “delta approach” of applying the climate signals from the climate models directly to observed series is still popular chiefly because of its simplicity and the need for less data; only one variable is required. The perturbation delta approach is a combined downscaling method, combining the advantages of dynamical with statistical downscaling methods. It is the most common used method to transfer the signal of climate change from climate models to hydrological models [Bultot et al, 1988; Vehviläinen and Huttunen, 1997; Lettenmaier et al, 1999; Middelkoop et al, 2001]. There have been improvements on the approach by examining various scenarios to address the demerits of the method; but there still remains a challenge of simulating changes in extremes. This study uses a variant of the delta approach which exploits the merits while improving on some of the demerits. Instead of using simple change factors, the changes in extremes and changes in wet days are explored. The changes are extracted form the RCMs and then probabilistically applied to a given series.

The differences in the most relevant climatic variables to hydrology, typically rainfall and ETo, are extracted from the control simulations (simulations of the past and present climate) and the scenario

simulations (simulations of the future climate) of the climate model, and then applied to an observed input series of the hydrological model. The hydrological responses before applying the perturbations and after applying the perturbations determine the future climate change impacts. A schematic illustration of this modelling chain is shown in.Figure 18.

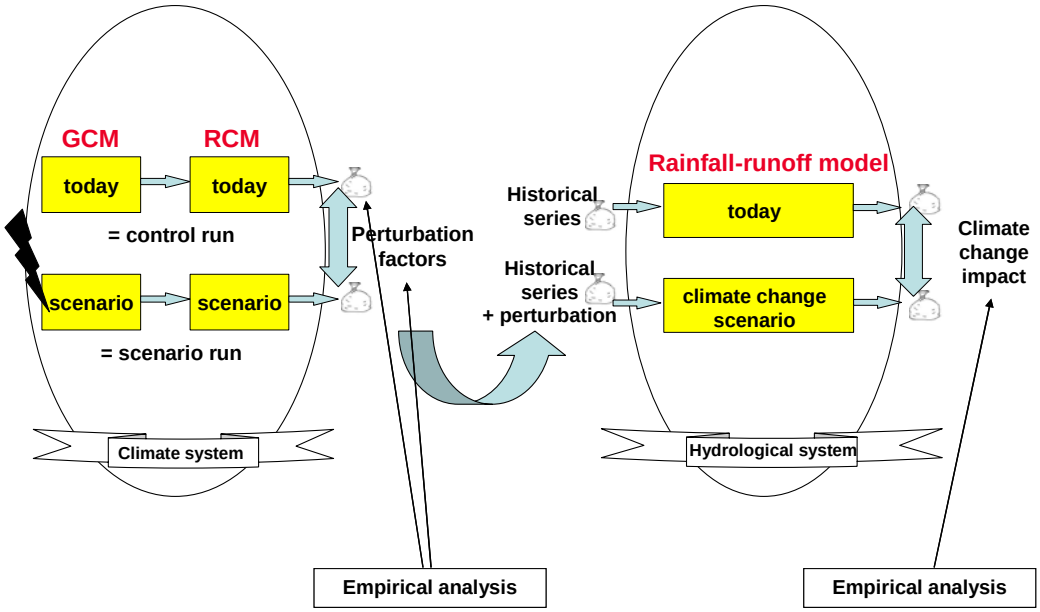

Figure 18: Schematic illustration of the standard “delta approach”.

The developed downscaling approach entailed perturbations for the number of wet days and perturbations for the rainfall intensity on a wet day. The combined effect of these two perturbations leads to perturbations on the rainfall intensity for given aggregation levels. These perturbations were also studied for different aggregation levels and return periods. The latter requires the perturbation factors to be calculated for quantiles (intensities or events with a specific probability level, or rank number after having sorted the events in a series with given length) applying a frequency analysis method. After having done so, climate change scenarios can be represented by changes in the probability distributions, the extreme value distributions, the cumulative volumes, or summarized by changes in intensity/duration/frequency (IDF) relationships. An overview of the downscaling approach and related outcomes is shown in Figure 19.

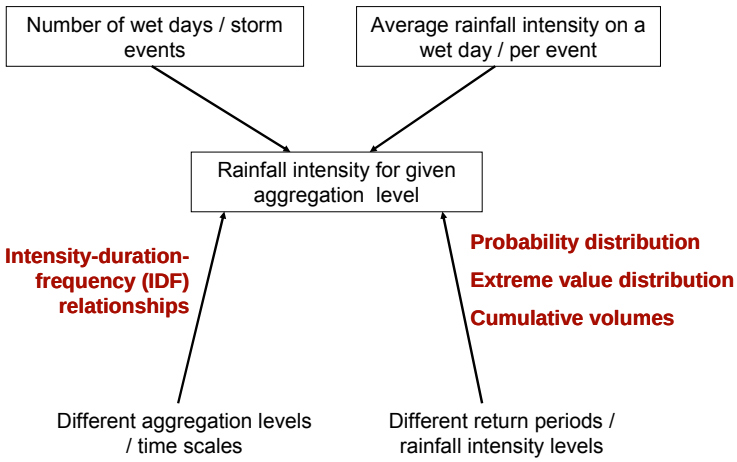

Figure 19: Downscaling approach and related outputs.

6.1 Transferring the climate change signal

The challenge still remains as to how end users can make use of a large set of models. The available simulations yielded different outputs. Ensemble techniques are currently being widely examined by climate scientists as the convergence of results from many models would not only increase confidence but also pave way for sharing information for future adjustments. This study borrowed some concepts of ensemble modelling by making use of the probabilistic perturbations derived from the selected PRUDENCE RCMs. The set of the 28 model results (from selected RCMs) implied that there were 28 possible scenarios which required close examination as all were equally plausible. Particular attention was paid to the wet day frequency perturbation, and the wet day intensity perturbation. The two perturbations are considered crucial for hydrological impact analysis. The use of probabilistic techniques ensured that the expected outputs represented the spectrum of all the projections. It is worth noting that no distinction was made on the different scenarios (A2 and B2) as there were few B2 scenarios compared to A2. Even so, there appeared to be no significant differences when observing the entire range of perturbations.

Thus far, Chapter 5 indicated that the wet days will get wetter and the dry days will get drier. Moreover, it is found in the project (see next) that during winter the wet days will generally increase in intensity, and the number of wet days will not significantly increase; although the number of wet days in summer will decrease. Also, it has been predicted that the intensity during both winter and summer will increase. The thunderstorms in summer may become more intense while the intensity on lower events may even decrease. These rainfall characteristics can be checked for similarities from the perturbations in wet day frequency and perturbations in the intensity of the wet days. The wet day for this study was taken as a day with rainfall higher than 0.1 mm. The study considered only the number of wet days and the wet day intensities as they are relevant for extreme frequency analysis. It is notable that despite the RCM biases in the number of wet days and intensities, the climate change perturbations tend to be closer to one another, hence increased confidence in the climate change signals.

6.1.1 The wet day frequency perturbation

The perturbation analysis focused on monthly grouped data to capture the intrinsic daily changes within each month. The analysis could also have been done at a seasonal scale but that would lead to less realistic results due to the coarse nature of the seasons. The change in wet days was calculated as a ratio of the number of wet days in a given month during the control period (1961-1990) to number of wet days during the corresponding month in the scenario period (2071-2100). Based on the n(=28) available model simulations the calculation was repeated implying that for each month there were n wet day perturbations. The range of results represented the overall uncertainty. The variability of the results suggested that probabilistic ensemble methods were required.

By making use of the normal probability characteristics, three scenarios were defined. The use of the normal distribution is pertinent because the changes reasonably fit the normal distribution. The high, mean and low estimates were extracted from the array of the number of wet day perturbations using the 95% confidence intervals. The upper confidence limit defined the high scenario while the lower confidence limit defined the low scenario. The mean scenario was represented by the mean of all the projected changes in the number of wet days. The developed scenarios would essentially subsume all the model projections for the changes in the number of wet days. In essence, pseudo models are derived that can suitably represent the entire range of projections. This reduces on the calculation time and makes the interpretation of the results easier since the amount of data is also reduced.

Figure 20 shows the model scenarios and the normal distribution scenarios selected for high, low and mean. The high, mean and low changes based on changes of individual models have a thinner range compared to the normal distribution range. Using individual models would lead to lower or higher estimates of the perturbations for some months. Consequently, it would fail to represent the whole range of expected changes.

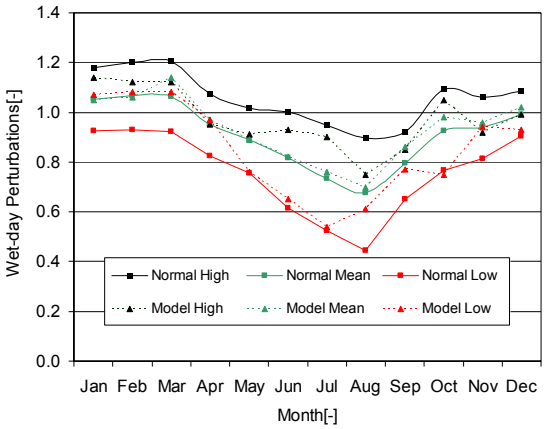

Figure 20: Perturbation on the number of wet days. High, mean and low scenarios are calculated based on 95% confidence limits of a normal distribution (normal high, normal mean, and normal low). Selected high, mean and low models are also shown.

6.1.2 Quantile perturbations

In addition to the wet day frequency perturbation, the perturbation on the intensity is necessary. The method selected was based on the principles of the quantile-perturbation method. The perturbations are calculated based on a frequency analysis by comparing ranked daily extremes in the control period to ranked daily extremes in the scenario period. The perturbations are then statistically assessed based on the normal distribution. For any given recurrence interval, there are n (28 models) possible perturbations which generally fit the normal distribution. Therefore, a perturbation pattern can be traced by combining all the intensity perturbations with similar probabilities of exceedance. To elaborate further, for a normal distribution, the 95% confidence limits can be defined for each exceedance probability (recurrence interval) after which a pattern can be traced through the limits to produce a curve representing a scenario changes. This traced curve can then be used to interpolate the intermediate recurrence intervals and to smoothen the intensity perturbation versus recurrence interval. This is particularly important when transferring the perturbation to an observed series. The exceedance probability is calculated relative to the wet days within the series.

Figure 21 shows the quantile-perturbation plot for the PRUDENCE RCMs. The months selected represent the typical perturbation variability during summer (July) and winter (January). During the winter months, the perturbations are fairly invariable with exceedance probability for most of the models. However, during summer, the perturbations are dependent on the exceedance probability with the higher extremes having higher perturbations. During winter, the extremes are expected to increase uniformly while the summer high extremes will be more intense. The high, mean, and low boundaries have also been superimposed in Figure 21. The three frequency-perturbation boundaries prescribe the ensemble changes required to represent the entire range of the projections.

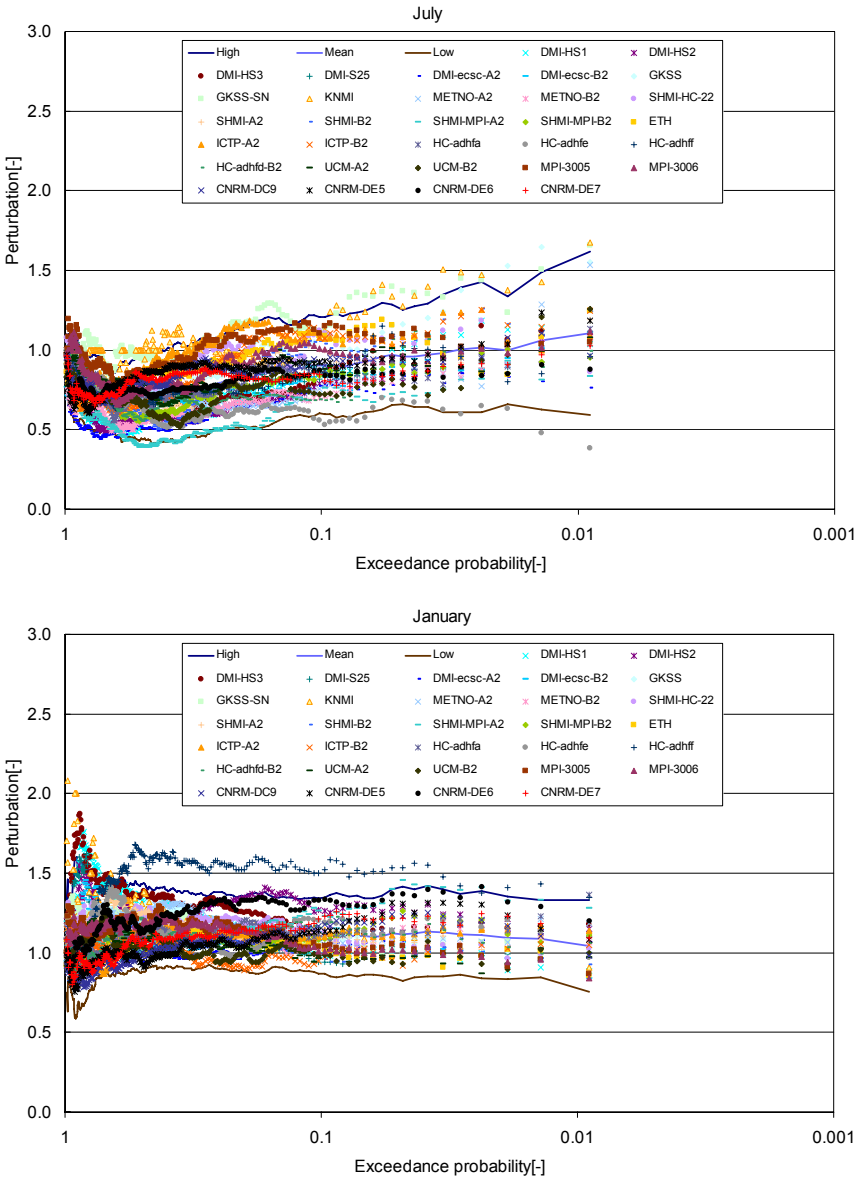

Figure 21: Typical wet day quantile-perturbation projections for summer (July) and winter (January). The high, mean and low scenarios are based on the normal distribution (95% confidence limits) and represent the range of the perturbations.

6.2 Time series climate change perturbation for rainfall

The time series perturbation is essential for climate change impact analysis. The mismatch between the RCM model results and the observations suggests that direct input of the climate data leads to misleading results. The alternative would require an indirect approach which involves extracting the climate change signal from the climate model outputs and applying this signal to the observed series to reproduce the climate change impact. The time series perturbation is essentially a two step process (Figure 22). The climate change signal mainly contains a wet day frequency signal, and an intensity signal. The wet day frequency signal signifies the changes in the number of wet days while the intensity signal represents the changes in the magnitude of the extremes. The array of models implies that several signals are available and all are likely. As previously stated the signals were derived from the normal distribution for the high, mean, and low representing the entire range of results for both the wet day and intensity perturbation. First, the number of wet days to be added or removed is determined for the high, mean and low perturbations. The wet day correction is applied through a random procedure for the three cases (high, mean, and low). When adding wet days, the wet days are randomly selected from the set of empirical wet days of the observed series and added to dry days. When removing the wet days, the wet days are also randomly selected but are equated to zero.

Second, the intensity perturbation for high, mean, and low is applied to the series. The final series now represent a high, mean and low climate change series.

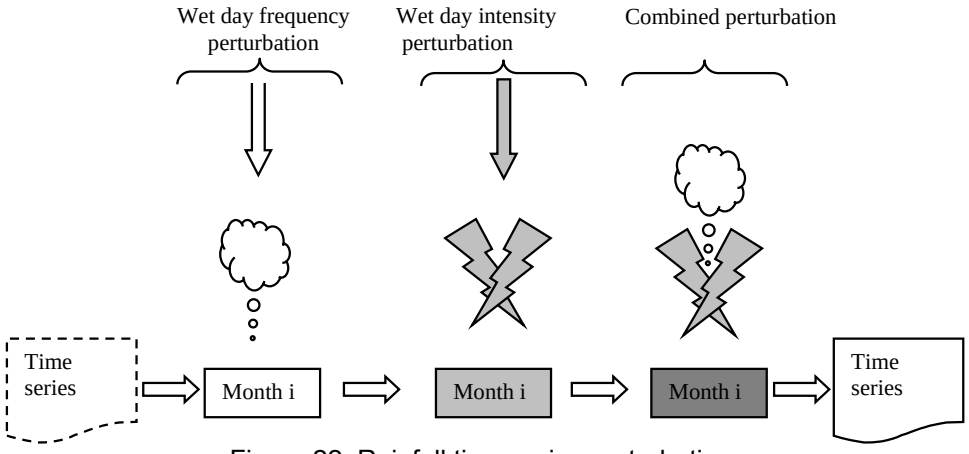

Figure 22: Rainfall time series perturbation.

6.3 ETo series perturbation

ETo is one of the important input parameters for hydrological models. The climate change transformation for ETo is not practiced widely. Most researchers transform the ETo series by applying a mean perturbation factor; others also use a mean series that is invariable with time. This is justified by the inherent low inter-annual variability of ETo. The future ETo rates, however, considerably differ from the current ETo rates which undermines the use of mean temporally invariant ETo rates. The future variability of ETo is still unclear but temperatures may be used as precursors of ETo rates. Only temperature is reasonably modelled by climate models; the other variables have a high uncertainty. ETo can thus be calculated from the temperature data but for a humid climate extra information is required (wind speed and relative humidity) for a better estimation of the ETo changes. However, this is still difficult as the climate models poorly model variables necessary for investigating ETo. Nonetheless, impact analysis can proceed with the available data. The methodology of rainfall perturbation is preferred here albeit for only the intensity perturbation. This involves comparing the ordered control series and the scenario series through frequency analysis.

The intensity perturbation was also analysed on a monthly basis similar to the rainfall series. The perturbations in winter are fairly constant with exceedance probability implying that the extremes in winter increase uniformly. Summer, however, shows unstable perturbations for the high frequency values (Figure 23). These perturbations are likely unrealistic as the models have been found to have excessive drying within the soil-water models of the RCMs. Thus, there is little confidence in the extremely high perturbations for the high frequency values. Indeed these models affect the high, mean, and low scenario perturbation curves which are generated from a normal distribution. The shape of the perturbation pattern is affected by the anomalous values. The Hadley centre models form the majority of the models with sharp bends in the perturbation factors (HC-adhfe, HC-adhff, and HC-adhfd-B2). Compared to summer, the winter perturbations were more stable considering the range of the recurrence intervals. The high, mean, and low scenarios were extracted using the normal distribution. These are then used in the time series perturbation of the ETo series. The high, mean and low intensity perturbations are applied to an observed ETo series to generate three ETo time series for the future climate.

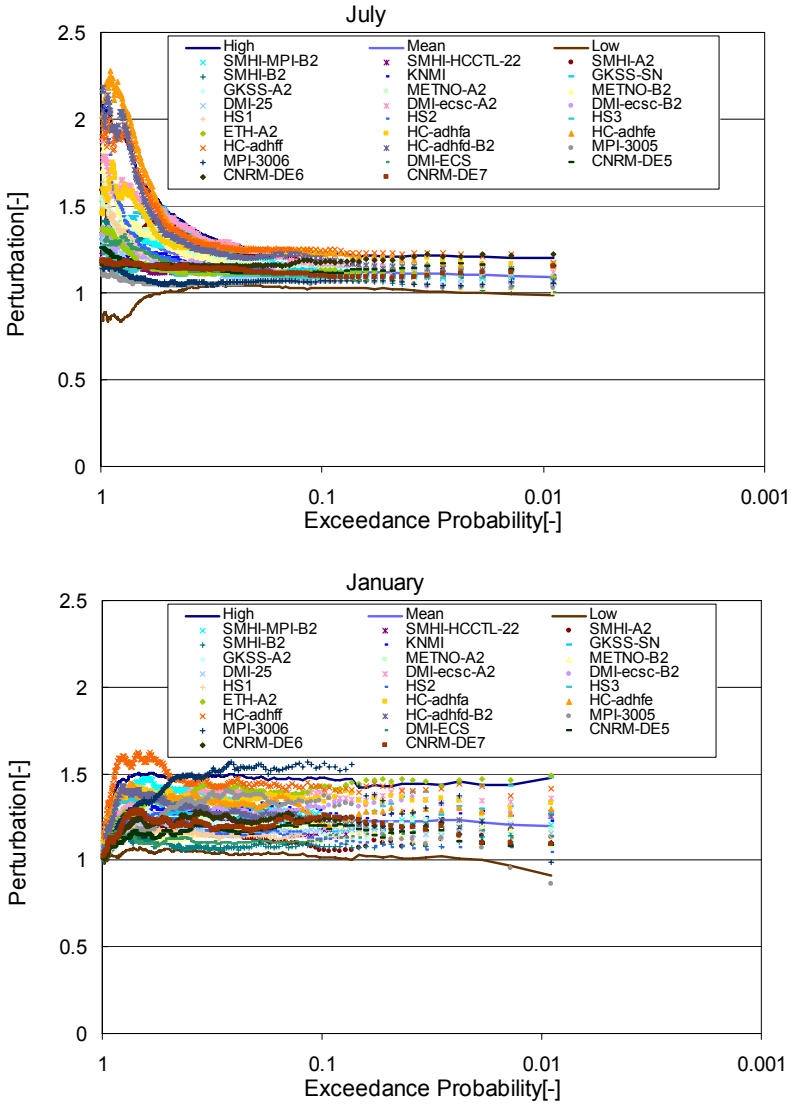

Figure 23: Typical daily ETo quantile-perturbation projections for summer (July) and winter (January). The high, mean and low are based on the normal distribution (95% confidence limits) and represent the range of the perturbations.

6.4 Transformation of rainfall and ETo series for impact analysis

Hydrological impact analysis depends on the inputs of rainfall and ETo. The perturbations of ETo and rainfall are done concurrently to preserve the internal physics of the climate system. For each month three rainfall and ETo series are available for the high, mean, and low scenarios. However, it is not clear whether a high rainfall perturbation (implicit for a high flood impact) should be combined with a high ETo perturbation. In other words, an investigation into the possible correlations between the two variables is necessary. Regression analysis was performed to identify the relationships between rainfall and ETo. The aim of this analysis was to infer what combinations of rainfall and ETo perturbations are physically meaningful. To elaborate further, it would be important to investigate the seasonal relationships of the perturbations. For instance, whether a model with high rainfall perturbations in winter also projects high perturbations in ETo and what projections for rainfall and ETo this model gives for other seasons. To deduce these relationships, the perturbations of the same models would be traced across all the seasons. The relationships would then be used to define the impact scenarios: high, mean and low. The high impact scenario is explained by high rainfall perturbations (mainly during winter) while the low impact scenario is associated with the low rainfall perturbations.

The quantile perturbation method was performed on the daily seasonal values and average perturbations were then estimated (return period > 0.1 year) for both rainfall and ETo. Since each

model has data for rainfall and ETo, a perturbation correlation analysis is possible. Figure 24 shows the ETo-rainfall perturbations for the four climatological seasons. The possible combinations can now be identified by observing the behaviour of the same models across all the seasons. By classifying models as high, mean and low based on the winter season, the perturbations of the same models in spring, summer, and autumn suggest the potential combinations of ETo and rainfall. The categorisation of the perturbations as high, mean, and low is based on the range of values. This classification is made for the two variables: ETo and rainfall. The high rainfall perturbations in winter appeared to be followed by low rainfall perturbations in summer. Summer perturbations for the same winter high models appeared to predominantly be located in the lower half of the rainfall perturbations. The ETo perturbations appeared to be high for both the winter and summer. Similarly, the mean and low scenarios were derived. It is apparent that for the transitional seasons (spring and autumn), relationships are difficult to ascertain from the correlations alone meaning that several trials are investigated to infer the combinations. For the main seasons, it was clearer albeit not obvious. With the developed combinations, an observed series can now be perturbed to generate three scenarios that would represent the range of expected climate change.

Table 7 illustrates the combinations that were found to realistically represent the range of RCM impact perturbations. The scenarios are classified as high, mean, and low because of the expected impacts. With each month having a high, mean, and low rainfall and ETo series, the combinations in

Table 7 are crucial for compiling the series for impact analysis. For the high impact scenario, the rainfall series can be compiled by selecting the high rainfall (highest perturbations) for winter months, low rainfall (lowest perturbations) for the summer months, and mean rainfall (mean perturbations) for the spring and autumn months. Using a similar approach, the ETo high series is perturbed. The two series are then input in a hydrological model to simulate the high impact scenario. The same procedure is followed to derive rainfall and ETo series for the mean and low impact scenarios. The range of impacts is then estimated from the three scenarios.

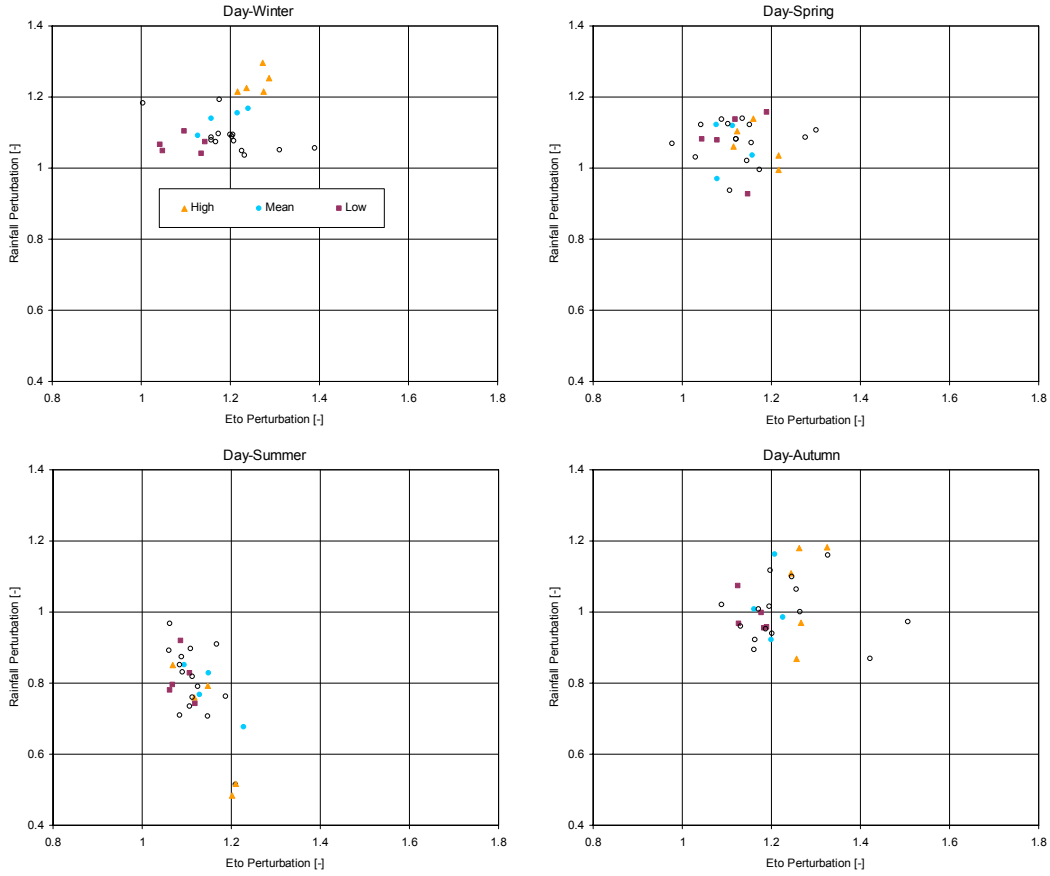

Figure 24:Climatological seasons correlation analysis for determining the potential ETo and rainfall combinations. The perturbations are classified as high, mean, and low based on the winter season. The triangles (high), full circles (mean), and the squares (mean) represent the same models across the four seasons. The empty circles represent models that were excluded from the classification.

Table 7: Seasonal correlations and scenario definition (climatological seasons)

Season	ETo	Rainfall	Scenario
Winter	High	High	High
Spring	Mean	Mean	
Summer	High	Low	
Autumn	Mean	Mean	
Winter	Mean	Mean	Mean
Spring	Mean	Mean	
Summer	Mean	Mean	
Autumn	Mean	Mean	
Winter	Low	Low	Low
Spring	Low	Mean	
Summer	Low	Low	
Autumn	Low	Mean	

6.5 Scenario scaling factors

The PRUDENCE project mainly provides regional data for the SRES A2 and B2 scenarios. By definition, the A2 scenario is considered a medium-high scenario while the B2 scenario is taken as a medium-low scenario. These scenarios account for a limited range of the projections. Other scenarios are required to estimate the expected range of impacts for all the scenarios including the high scenarios (A1) and the low scenarios (B1). Due to various constraints, only a few scenarios from regional climate models exist to date but there are many available scenarios from global circulation models, which can provide a basis for estimating regional factors. By applying scaling factors, impacts for emission scenarios not available at regional scale can be estimated. A simple approach involves a comparison of both the GCM and RCM estimates. The scaling factor is derived by comparing the range of perturbations of the RCMs to the range of perturbations of the GCMs (including additional scenarios).

From the IPCC AR4 data base (Table 3), rainfall series for the A1B, A2 and B1 scenarios were extracted. The monthly data from the database were analysed to estimate the seasonal perturbations for all the scenarios. The seasonal scale factors were preferred because at a seasonal scale it was expected that for the same scenario the projected changes for RCM based scenarios would fairly match those of the GCM based scenarios. Since both global and regional scenarios have a common A2 scenario, the scaling factor is calculated as a ratio based on A2. By comparing the seasonal GCM data for the A2 scenario and the seasonal RCM data for the A2 scenario, it was established that the seasonal factor ranges are similar for both the summer season and the winter season. It is important to keep in mind that the A2 high, mean and low factors from the RCMs are expected to be mirrored with the A2 high, mean, and low factors for the GCMs.

Due to the adopted methodology for impact analysis which requires an estimate of the high, mean, and low scenarios, 3 scaling factors were derived. Figure 25 shows the three factors for the RCMs (solid lines), and GCMs (dash lines).

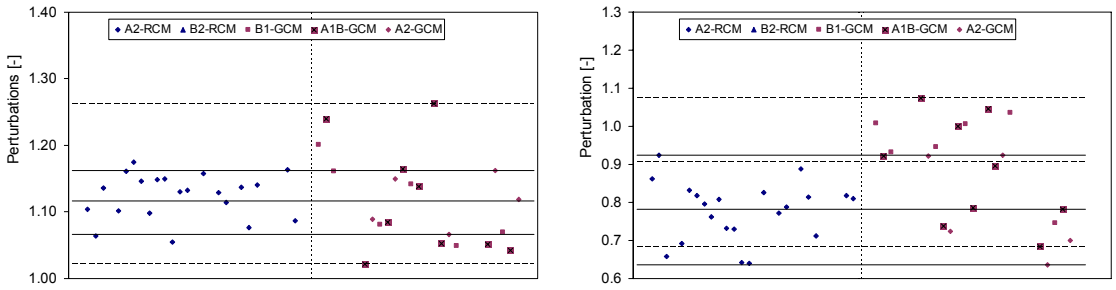

Figure 25: Scaling factor estimation from RCMs and GCMs for winter (right) and summer (left). Seasonal perturbations for the RCMs are shown on the left and the GCM perturbations are shown on the right.

The RCM high, mean and low factors were calculated from only the A2 and represent the scenarios at regional scale. The GCM high, mean and low factors were calculated from the other scenarios (A1B and B1). Given the GCM high, mean, and low scenarios H_g, M_g, and L_g and the RCM high, mean and low scenarios H_r, M_r, L_r the corresponding scaling factors would be H_g/H_r, M_g/M_r and L_g/L_r. These factors are calculated for both seasons: the hydrological summer and winter seasons. They are then applied to the time series at a seasonal scale; all the months of summer and winter would be multiplied by the corresponding factor. Scaling factors were higher during the summer season with winter showing low changes (< 10%). The inclusion of more scenarios (A1B and B1) in the GCM predictions creates a significant difference in summer. The factors for summer were positive (Table 8) but the low scaling factor was not realistic as it would increase the RCM low higher than the A2 scenario thus the previous RCM low was retained hence the scaling factor of 1.

Table 8: Seasonal scaling factors to account for extra scenarios A1B, B1

Season	High	Mean	Low
Winter	1.09	1.00	0.96
Summer	1.16	1.16	1.08 (1)

7 General conclusions from Phase 1

During Phase 1 of the CCI-HYDR project both the theoretical and practical contexts of the climate change impacts on hydrological extremes were established. The theoretical contexts involved literature studies that were influential in understanding the past and future changes in the Belgian climate. The practical context involved applying the extracted changes from the GCMs to the hydrological models. This required a range of statistical techniques especially aimed at capturing the spectrum of future projections.

The historical analysis was primarily based on long term rainfall and evapotranspiration observed series. It was established that the rainfall patterns showed deviant behaviour from the long term average during periods of 30-40 years. However, the evidence of cyclic behaviour is not strong due to the limited length of the series (108 years for rainfall). Nonetheless, there is a reason to be concerned as the recent significant trends suggest. The potential evapotranspiration analysis also revealed significant features, albeit not as evident as in rainfall. However, like rainfall, the winter season showed the highest changes for the most recent decade. Summer and spring showed somewhat insignificant changes but autumn displayed positive significant behaviour for evapotranspiration.

The PRUDENCE models were found to be realistic for regional studies in Belgium. Despite the biases most of the models reproduced realistically the meteorological characteristics of the climate in Belgium. However, temperature was simulated better than rainfall which was expected as GCMs have been found to be better at modelling temperature than the intermittent rainfall. The selected PRUDENCE models exhibited both negative and positive changes (-40% to +10%) in rainfall during summer, and positive changes during winter (+5% to +50%). With the exception of the coastal region, there were no other significant regional differences in the climate change signals over Belgium. The Belgian coastal region showed on average 15% higher perturbation factors during the winter and summer periods than the rest of the country.

A climate change Excel based algorithm has been developed for the end users. It generates the three scenarios for high, mean, and low. This will enable the end users and more especially the impact modellers to apply the downscaling technique and generate time series relevant to a particular region.

8 Future research

Future research will primarily deal with impact modelling towards flood risk and low flows using hydrological and coupled hydrological-hydrodynamic river models. Flood risk will be assessed for urban drainage systems by considering the impact on sewer flood frequencies and magnitudes, combined sewer overflow frequencies and receiving river impact for selected systems. Flood risk and low flows will be investigated for rivers.

Finally, the implications of the changes in flood and drought risks will continue to be investigated through a collaboration with the ADAPT project. The implications to society, water mangers and policy makers will be assessed.

It is important to note that this project report summarises 2 years of research (Phase 1) which means that some details may appear incomplete or unclear. The reader is directed to the project website (http://www.kuleuven.be/hydr/CCI-HYDR.htm) for the more detailed reports.

9 References

Blanckaert, J. and P. Willems (2006), Statistical analysis of trends and cycles in long-term historical rainfall series at Uccle, paper presented at the 7th International Workshop on Precipitation in Urban Areas, St.Moritz, Switzerland.

Bultot, F., Coppens, A., Dupriez, G. (1983), 'Estimation de l'évapotranspiration potentielle en Belgique', Publications/publicaties série/serie A, No/Nr 112, Institut Royal Météorologique de Belgique - Koninklijk Meteorologisch Instituut van België , 28 p.

Bultot, F., Coppens, A., Dupriez, G.L., Gellens, D., Meulenberghs, F. (1988a), 'Repercussions of a CO2 doubling on the water cycle and on the water balance – A case study for Belgium', Journal of Hydrology, 319-347.

Bultot, F., Dupriez, G.L., Gellens, D. (1988b), 'Estimated annual regime of energy-balance components, evapotranspiration and soil moisture for a drainage basin in the case of CO2 doubling', Climatic Change 12 (1988) 39-56.

Casty, C., H. Wanner, J. Luterbacher, J. Esper, and R. Böhm (2005), Temperature and precipitation variability in the European Alps since 1500, International Journal of Climatology, 25(14), 1855-1880.

Christensen JH, Carter TR, Rummukainen M (2007), Evaluating the performance and utility of regional climate models: the PRUDENCE project. Clim Change, doi:10.1007/s10584-006-9211-6.

Christensen, JH. (2005), Prediction of Regional scenarios and Uncertainties for Defining EuropeaN climate change risks and Effects. PRUDENCE Final Report, available from http://prudence.dmi.dk/public/publications/

De Jongh, I. L. M., N. E. C. Verhoest, and F. P. De Troch (2006), Analysis Of A 105-year time series of precipitation observed at Uccle, Belgium, International Journal of Climatology, 26(14), 2023-2039.

Gellens, D., Roulin, E. (1998), 'Stream flow response of Belgian Catchments to IPCC Climate change scenarios'. Journal of Hydrology 210 (1998) 242-258.

IPCC (2001), Climate change 2001: the scientific basis, contribution of Working Group I to the Third Assessment Report of the Intergovernmental Panel on Climate Change. In: Houghton JT et al (eds).Cambridge University Press, Cambridge, UK, pp 881.

Lettenmaier, D. P., Wood, A. W., Palmer, R. N., Wood, E. F., and Stakhiv, E. Z. (1999), Water Resources Implications of Global Warming: A U.S. Regional Perspective, Clim. Change 43, 537–579.

Lombard, F. (1988). Detecting Change-points by Fourier Analysis. Technometrics, 30, 3, p. 305-310.

M.J.M. de Wit, B. van den Hurk, P.M.M. Warmerdam, P.J.J.F. Torfs, E. Roulin and W.P.A. van Deursen (2007),, Impact of climate change on low-flows in the river Meuse, Climatic Change 82 pp. 351–372.

Middelkoop H, Daamen K, Gellens D, Grabs W, Kwadijk JCJ, Lang H, Parmet BWAH, Schädler B, Schulla J, Wilke K. (2001), Impact of climate change on hydrological regimes and water resources management in the Rhine Basin. Clim Change 49:105–128.

Ntegeka, V., and P. Willems (2008), Trends and multidecadal oscillations in rainfall extremes, based on a more than 100 years time series of 10 minutes rainfall intensities at Uccle, Belgium, Water Resour. Res., doi:10.1029/2007WR006471, in press.

Pettitt, A. N. (1979). A Non-parametric approach to the Change-point Problem. Appl. Statist. 28, 2, p. 126-135.

Räisänen, J., Hansson, U., Ullerstig, A., Döscher, R., Graham, L.P., Jones, C., Meier, H.E.M., Samuelsson, P., Willén, U. (2004), 'European climate in the late twenty-first century: regional simulations with two driving global models and two forcing scenarios', Climate Dynamics, 22, 13-31.

Roulin, E., Arboleda, A. (2002), 'Integrated modelling of the hydrological cycle in relation to global climate change - The Scheldt river Basin'. Complement to the Final Report of the project GC/34/08A in the framework of the « Global change and sustainable development » program of the Belgian Federal Services of Scientific, Technical and Cultural Affairs, 45 pp.

Roulin, E., Cheymol, A., Gellens, D. (2001), 'Integrated modelling of the hydrological cycle in relation to global climate change', Final Report of the project GC/34/08A in the framework of the « Global

change and sustainable development » program of the Belgian Federal Services of Scientific, Technical and Cultural Affairs, 62 pp.

Tukey JW. (1977), Box-and-Whisker Plots. In: Tukey JW,editor. Explanatory data analysis. Reading (MA): Addison-Wesley;. p. 39–43.

Türkes, M., U. M. Sümer, and G. Kiliç (2002), Persistence and periodicity in the precipitation series of Turkey and associations with 500 hPa geopotential heights., Climate Research, 21(1), 59-81.

Vehviläinen, B. and Huutunen, M. (1997). Climate change and water resources in Finland. Boreal Environment Research 2 3, pp. 3–18.